https://doi.org/10.5194/egusphere-2022-1229
Preprint. Discussion started: 6 December 2022
© Author(s) 2022. CC BY 4.0 License.

Multiscale meteorological controls and impact of soil moisture heterogeneity on radiation fog in complex terrain

Dongqi Lin[1,2], Marwan Katurji[2], Laura E. Revell[1], Basit Khan[3], and Andrew Sturman[2]

[1]School of Physical and Chemical Sciences, University of Canterbury, Christchurch, New Zealand
[2]School of Earth and Environment, University of Canterbury, Christchurch, New Zealand
[3]Institute of Meteorology and Climate Research, Atmospheric Environmental Research (IMK-IFU), Karlsruhe Institute of Technology (KIT), 82467 Garmisch-Partenkirchen, Germany

Correspondence: Dongqi Lin (dongqi.lin@canterbury.ac.nz)

Abstract. Coupled surface-atmosphere high-resolution simulations were carried out to understand radiation fog development and persistence in a city surrounded by complex terrain. The controls of mesoscale meteorology and microscale soil moisture heterogeneity on fog were investigated using case studies for the city of Christchurch, New Zealand. Numerical model simulations from the synoptic to micro- scale were carried out using the Weather Research and Forecasting (WRF) model and the Parallelised Large-Eddy Simulation Model (PALM). Heterogeneous soil moisture, land use, and topography were included. The spatial heterogeneity of soil moisture was derived using Landsat 8 (https://www.usgs.gov/landsat-missions/landsat-8, last access: 10 October 2022) satellite imagery and ground-based meteorological observations. Eight simulations were carried out under identical meteorological conditions. One contained homogeneous soil moisture and one contained heterogeneous soil moisture derived from Landsat 8 imagery. For the other six simulations, the soil moisture heterogeneity magnitudes were amplified following the observed spatial distribution to aid our understanding of the impact of soil moisture heterogeneity. Our results showed that soil moisture heterogeneity did not significantly change the general spatial structure of near-surface fog occurrence, even when amplified. However, compared to homogeneous soil moisture, spatial heterogeneity in soil moisture leads to significant changes in radiation fog duration. The resulting changes in fog duration can be more than 50 minutes, although such changes are not directly correlated with spatial variations in soil moisture. The simulations showed that the mesoscale (10^4 to 2×10^5 m) meteorology controls the location of fog occurrence, while soil moisture heterogeneity alters fog duration at the microscale (10^{-2} to 10^3 m). Our results highlight the importance of including soil moisture heterogeneity for accurate spatiotemporal fog forecasting.

1 Introduction

Dense fog has been identified as one of the greatest hazardous meteorological phenomena in the atmospheric boundary layer (ABL) (Duynkerke, 1991; Mason, 1982). Fog is a result of water droplets and/or ice crystals occurring in suspension near the Earth's surface, which limits visibility to less than 1 km (Brown and Roach, 1976; Gultepe et al., 2007; Steeneveld et al., 2015; WMO, 1992). Fog can be classified into several types based on the main driving meteorological processes (e.g. Gultepe et al., 2006; Tardif and Rasmussen, 2007; Van Schalkwyk and Dyson, 2013; Belorid et al., 2015; Bari et al., 2016; Roux et al., 2021;

https://doi.org/10.5194/egusphere-2022-1229
Preprint. Discussion started: 6 December 2022
© Author(s) 2022. CC BY 4.0 License.

Lin et al., 2022). For instance, advection fog is usually related to a moist warm air mass moving over a colder surface, while radiation fog is driven by more localised processes, particularly radiative cooling of the ground surface. The main focus of this paper is radiation fog. Among several thermal and dynamical processes in the ABL, land surface physical characteristics have been identified as the most important factors for fog formation (Duynkerke, 1991). The physical characteristics of the land surface, including land use, soil moisture, and soil temperature, have a significant impact on the coupled energy and water exchanges between the land surface and ABL (e.g. Bou-Zeid et al., 2004; Maronga et al., 2014; Rihani et al., 2015; Shao et al., 2013; Srivastava et al., 2020). Gultepe et al. (2007) pointed out that radiation fog over a heterogeneous land surface is difficult to forecast. The spatial heterogeneity in land-atmosphere interactions and surface energy balance can impact energy transfer between the atmosphere, ground surface, and soil (e.g. Courault et al., 2007; Huang and Margulis, 2013; Maronga et al., 2014). Here, we recognise heterogeneity as spatial variability in land surface characteristics, while homogeneity means characteristics are spatially uniform.

Over the past decade, many studies have included heterogeneous land surface characteristics in radiation fog simulations in order to understand the microscale processes (occurring from 10^{-2} to 10^{3} m, and from seconds to hours) and associated feedback during fog development. High resolution numerical weather models, including Large Eddy Simulation (LES) models, are useful tools for improving the understanding of dynamical processes involved in the radiation fog life cycle within a complex environment. With higher resolution, the microscale processes related to surface heterogeneities can be better resolved and represented. Bergot et al. (2015) investigated the impact of the heterogeneously built environment over flat terrain at Paris–Charles de Gaulle airport, while Mazoyer et al. (2017) demonstrated the impact of a plant canopy on a radiation fog event observed during the ParisFog field campaign (Haeffelin et al., 2010). Both studies applied simulations at grid spacings $\leq$ 5 m using an LES model and found that variations in land use lead to spatial heterogeneities of fog.

While numerical simulations at metre-scale are highly valuable, they are also highly computationally expensive. In the last few years, to compromise between computational cost and simulation scale, several studies have carried out simulations over complex heterogeneous topography at sub-km scale (with grid spacing of a few hundred metres). For example, Bergot and Lestringant (2019) carried out a case study with two horizontal numerical grid spacings (500 m and 50 m) in a north-eastern region of France. Ducongé et al. (2020) conducted simulations with 100 m horizontal grid spacing in the Shropshire hills (UK), and Smith et al. (2020) applied sub-km simulations (1.5 km, 333 m, and 100 m) over the Cardington and Shropshire regions. All these studies highlighted that even over a relatively small area (less than 4 km^2), when a complex and heterogeneous environment is present, fog occurrence and type can vary significantly.

In addition to topography, soil moisture is identified as an important attribute of land surface characteristics. Changes in soil moisture lead to variability in the surface energy balance, and consequently changes in fog duration. Maronga and Bosveld (2017) investigated the impact of perturbations in soil moisture at model initialisation on radiation fog, and found that such perturbations only affect the lifting and dissipation of the fog layer, while fog formation time was not impacted. They highlighted that drier soil was associated with more energy at the surface contributing to greater surface sensible heat flux. As a consequence of increased surface sensible heat flux, the rate of surface heating increased leading to earlier dissipation of the fog layer. However, Maronga and Bosveld (2017) only conducted their simulations over grassland with flat terrain and

https://doi.org/10.5194/egusphere-2022-1229
Preprint. Discussion started: 6 December 2022
© Author(s) 2022. CC BY 4.0 License.

homogeneous soil moisture. Smith et al. (2020) included complex topography and demonstrated the impact of soil thermal conductivity and different choices of land surface parameterization on fog formation, dissipation, and duration. Temperature biases were found in the heterogeneous hill and valley structures, with simulated temperatures over hills being too cold leading to too much fog, while the temperatures over the valleys were too warm leading to too little fog. In addition, they showed that fog formation time is highly sensitive (4 hours difference) to soil and land surface parameterizations, while dissipation time is relatively insensitive (1.5 hours difference at most). These aforementioned numerical modelling studies usually only included one component of the land surface heterogeneity. Bergot et al. (2015) and Mazoyer et al. (2017) conducted their simulations using flat topography with homogeneous soil moisture. Maronga and Bosveld (2017) conducted an idealised study with homogeneous soil moisture, land use, and topography. The aforementioned studies (Bergot and Lestringant, 2019; Ducongé et al., 2020; Smith et al., 2020) that included complex mountainous environments usually did not consider effects of heterogeneity in land use or soil moisture. Therefore, the impact of soil moisture heterogeneity on radiation fog remains largely unknown.

Despite numerous fog studies worldwide, only a small number have been carried out for Christchurch (or, for that matter, New Zealand) (e.g. Lin et al., 2022; Osborne, 2002; Hume, 1999). Christchurch (43.5321° S, 172.6362° E) is located on the Canterbury Plains, on the east coast of the South Island, New Zealand (Figure 1). The city experiences fog events on approximately 44-49 days per year (Macara, 2016; New Zealand Meteorological Service, 1982). As the largest city of New Zealand's South Island, it is a vital port for aviation, shipping and surface transport. Hence, an accurate fog forecast is important for Christchurch and its international airport. Although Christchurch is a moderate-sized city (area of 1,426 km^2), great spatial heterogeneity exists in its land surface characteristics, which makes accurate fog forecasting difficult. Mesoscale flow systems are modified by the Southern Alps (highest peak elevation of 3754 m) to the west and Banks Peninsula (highest peak elevation of 920 m) to the south. An example of the impact of local flow phenomena (in this case mesoscale in nature) is when westerly flows passing over the Southern Alps interact with the north-easterly airflow along the coast, creating a wind convergence zone over Christchurch (e.g. Corsmeier et al., 2006; Sturman and Tapper, 2006). At nighttime, local airflow is also affected by cold air drainage from both the foothills of the Southern Alps and the Canterbury Plains to the west and the Port Hills on the southern boundary of the city. In the Christchurch area, radiation fog is the predominant type of fog, and radiation fog events usually coincide with stagnant air zones generated by local drainage flows (Lin et al., 2022).

In order to include forcing from local circulation and/or the terrain-induced drainage flows, the domain size of the simulations should be of the order of a few tens of kilometres (Ducongé et al., 2020), while several LES fog simulations at metre-scale have usually had a domain size less than 1 km (e.g. Bergot et al., 2015; Maronga and Bosveld, 2017; Schwenkel and Maronga, 2019). Considering the high computational cost, the optimal approach is to carry out high-resolution mesoscale simulations (Cuxart, 2015) at sub-km grid spacing. The surface and topographic heterogeneities can be partially resolved in such high-resolution mesoscale simulations, and consequently the dynamical processes and spatial variability of fog can be captured (Vosper et al., 2013, 2014). This study therefore aims to investigate the impact of soil moisture on radiation fog duration using high-resolution mesoscale simulations for Christchurch. In addition, we want to identify the meteorological controls that may be relevant for fog forecasting. The main objectives of this study are therefore to:

1. investigate the major meteorological controls on radiation fog in the complex environment of Christchurch

https://doi.org/10.5194/egusphere-2022-1229
Preprint. Discussion started: 6 December 2022
© Author(s) 2022. CC BY 4.0 License.

2. investigate the impact of soil moisture heterogeneity on radiation fog

A radiation fog scenario was created in numerical simulations with the finest grid spacing of 81 m. Data were obtained from numerous sources including meteorological observations and the Weather Research and Forecasting modelling system (WRF; http://www.wrf-model.org, last access: 17 May 2022). The fog simulations themselves were conducted using the Parallelised Large-Eddy Simulation Model (PALM) (Maronga et al., 2015, 2020). The WRF model is a state-of-the-art numerical atmospheric model that has high applicability in multiple world regions, and has been extensively used in numerous atmospheric and climate studies (Skamarock et al., 2021). PALM has been used for boundary layer studies for more than 20 years, including radiation fog studies in a stable boundary layer (Maronga and Bosveld, 2017; Schwenkel and Maronga, 2019). High resolution soil moisture data were derived from Landsat 8 imagery (at a resolution of 30 m) and used to construct experimental initial conditions of soil moisture in PALM. The experiments included a range of spatially heterogeneous soil moisture conditions in order to assess the impact of soil moisture on radiation fog duration.

2 Data and site description

Data sources used in this study are shown in Tables 1 and 2. To conduct PALM simulations, two types of input are important. One is the static driver, which includes geospatial data of land surface information and characteristics, such as topography, buildings, streets, vegetation, soil types, and water bodies. The other is the dynamic driver which contains the vertical profiles of the atmosphere and soil. The WRF simulations were initialised using data from the fifth generation of the European Centre for Medium-Range Weather Forecasts (ECMWF) atmospheric reanalysis of the global climate (ERA5) (Hersbach et al., 2019), and the WRF model configuration is identical to that described in Lin et al. (2021).

2.1 Geospatial data sets

As shown in Table 1, digital elevation model (DEM) and digital surface model (DSM) data were obtained from Environment Canterbury Regional Council (2020) for the major urban area of Christchurch. Both the DEM and the DSM have a spatial resolution of 1 m. The DEM provides information of ground surface altitude only, while the DSM includes the heights of all surface objects including buildings and trees. For areas outside of the major urban area, 1 m resolution DEM data are not available so we used a DEM with a spatial resolution of 25 m provided by Landcare Research (2018). No DSM is available outside of the main Christchurch metropolitan area. As we mainly focus on the area inside Christchurch, the 25 m DEM is sufficient to resolve the features and impacts of the surrounding areas. Land use information was obtained from Land Cover Database (LCDB) New Zealand (Landcare Research, 2020), while urban surface data, such as building outlines, streets and pavements were obtained from OpenStreetMap (https://planet.openstreetmap.org/; last access 14 April 2022). Land surface information and all geospatial data were included in the static driver input of PALM. In the static driver input files, the water temperature was set to 282.45 K based on the August mean of 2001 obtained from ERA5 reanalysis. The projection used for the static data is New Zealand Transverse Mercator (NZTM) - EPSG:2193. The static driver input files were created using a similar procedure to that described in Heldens et al. (2020) and Lin et al. (2021).

https://doi.org/10.5194/egusphere-2022-1229
Preprint. Discussion started: 6 December 2022
© Author(s) 2022. CC BY 4.0 License.

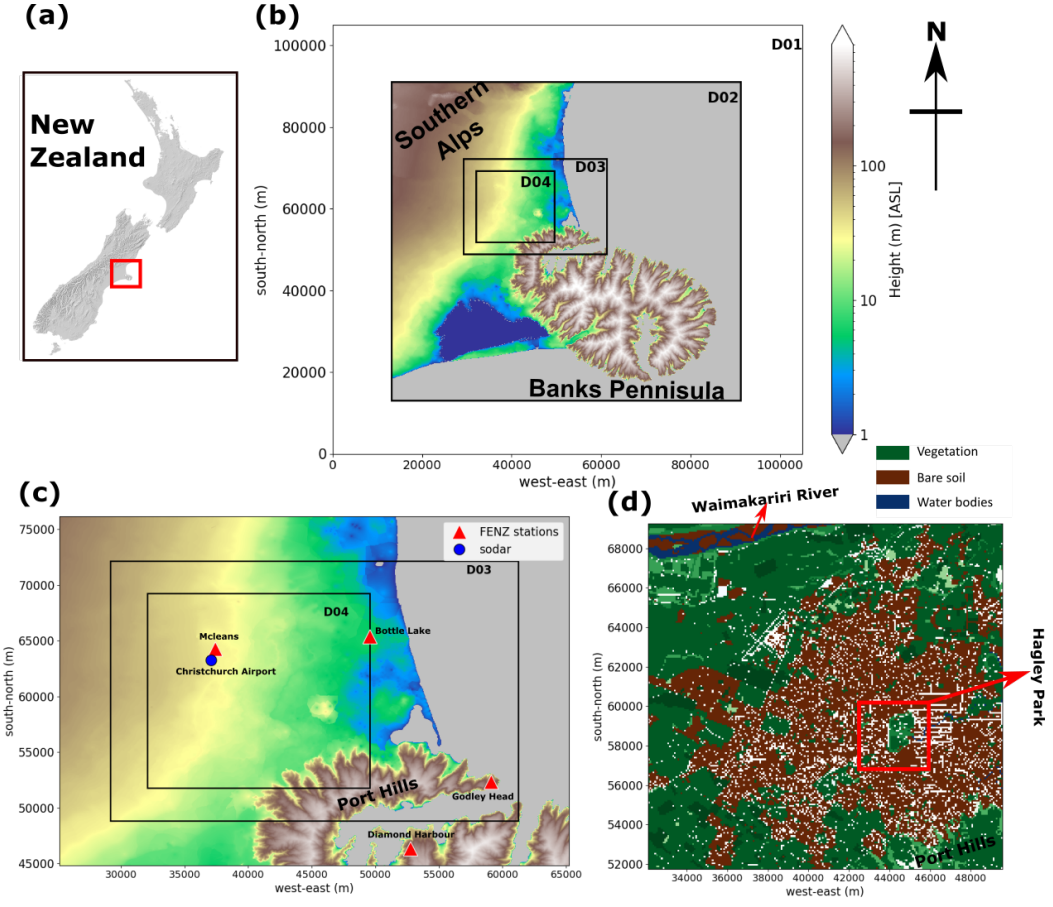

Figure 1. Maps and images of the case study simulation domains: (a) a New Zealand topographic map with a red square indicating the location of the simulation domains, (b) a topographic map (height above sea level) showing the simulation domain configuration for the case study, (c) a topographic map of simulation domains 3 and 4 (D03 and D04), the locations of the FENZ (Fire and Emergency New Zealand) weather stations, and the location of the sodar operated at Christchurch airport, and (d) a land use map of D04 with impervious areas (buildings, pavements, streets, etc.) in white. The simulation domain 1 (D01) configured as flat terrain with short grass, and hence no topography, is shown in panel (b). The logarithmic topographic height colormap in panel (b) applies to panels (b) and (c), while grey indicates the ocean.

2.2 Christchurch observational data network

One particular challenge of conducting fog research in Christchurch is its poor observational network. Despite being the second largest city in New Zealand, Christchurch has limited availability of meteorological observational data. Only the automatic weather station (AWS) operated at Christchurch International Airport (CHA) provides visibility measurements over the last 20 years. There are also no regular radiosonde launches in Christchurch, meaning no long-term vertical profiling data are available for investigation of the vertical structure of fog. In order to conduct radiation fog simulation using numerical models, vertical

https://doi.org/10.5194/egusphere-2022-1229
Preprint. Discussion started: 6 December 2022
© Author(s) 2022. CC BY 4.0 License.

Table 1. Sources and description of geospatial data sets used in this study.

Geospatial data		
Data set	**Source**	**Description**
Christchurch Digital Elevation Model (DEM) with spatial resolution of 1 m	Environment Canterbury Regional Council (2020)	Topographic height data for Christchurch city
Christchurch Digital Surface Model (DSM) with spatial resolution of 1 m	Environment Canterbury Regional Council (2020)	Data for Christchurch city, including altitude and height of surface geometries, such as buildings and trees
New Zealand South Island DEM with spatial resolution of 25 m	Landcare Research (2018)	Topographic height data for New Zealand South Island
New Zealand land cover database (LCDB) V5.0	Landcare Research (2020)	Land use categories for New Zealand
OpenStreetMap	https://planet.openstreetmap.org/ (last access: 14 April 2022)	Locations and outlines of buildings, pavements, and streets

profiles of the atmosphere before fog onset, and ground-based visibility observations are necessary. The former is required for PALM model initialisation, while the latter provides evidence of fog occurrence. Although atmospheric profiles can also be obtained from numerical weather prediction (NWP) models like WRF, the model simulation results still need to be validated using observational data.

The only available in situ observational campaign that satisfies the criteria took place from June to October 2001. An acoustic sodar was operated at CHA adjacent to an AWS which provides measurements of temperature, wind speed and direction, visibility, cloud height, etc. (Osborne, 2002). The vertical profiling data obtained from the sodar can also be used to identify the surface temperature inversion and hence verify radiation fog events. Although no radiosonde data are available for the sodar operation period, the national climate database (CliFlo; https://cliflo.niwa.co.nz/; last access: 21 October 2022) operated by the National Institute of Water and Atmospheric Research (NIWA), provides upper air measurements obtained from sensors on aircraft arriving at and departing from Christchurch airport. The data set includes measurements of temperature, wind speed and direction, pressure, and height. The measurement frequencies for temperatures and winds are every 12 hours and 6 hours, respectively, when aviation is not impacted by weather conditions.

During the entire sodar operational period (140 days), 24 days were associated with visibility less than 1 km. Based on the sodar observations, 6 radiation fog events were identified. Only the event that occurred at around 1700 UTC on 5th August 2001 has upper air measurements available before fog onset. These upper air measurements were available for 1200 UTC 5th August

https://doi.org/10.5194/egusphere-2022-1229
Preprint. Discussion started: 6 December 2022
© Author(s) 2022. CC BY 4.0 License.

Table 2. Sources and description of meteorological data sets used in this study.

Meteorological data		
Data set	**Source**	**Description**
ERA5	ECMWF	Meteorological input data for WRF simulation and water temperature in PALM simulations
Upper air observations	CliFlo (https://cliflo.niwa.co.nz/; last access: 21 October 2022)	Vertical profiles of wind, temperature, pressure, and measurement heights for PALM initialisation
Sodar observations	University of Canterbury, New Zealand	Radiation fog event identification and verification
Landsat 8 satellite soil observations	Sentinel Hub EO Browser (Sinergise Ltd, 2022a, b, last access: 14 April 2022)	Landsat 8 satellite imagery providing soil moisture heterogeneity pattern
Ground-based soil moisture content observations	New Zealand Modelling Consortium, Open Environmental Digital Library (https://envlib.org; last access: 21 October 2022)	Soil moisture content observational data obtained from Automatic Weather Stations (AWSs) operated by Fire and Emergency New Zealand (FENZ)

2001, 5 hours before fog onset, which is suitable for model initialisation. The time series of AWS and sodar observations, and the synoptic conditions for this fog event are shown in Appendix A. This particular fog event has characteristics that agree with those identified in a recent Christchurch fog climatology study (Lin et al., 2022). In Christchurch, winter (June, July, and August) has the highest frequency of radiation fog occurrence. Near-surface temperature inversions represent a key characteristic of radiation fog development, which is typically associated with sodar observations of an inversion layer situated between 50 m and 100 m above the surface (Figure A1). Both sodar and AWS observations show low wind speeds near the surface (Figure A1) during this event, indicating a calm and relatively stable near-surface layer. The ERA5 reanalysis of mean sea level pressure (MSLP; Figure A2) shows anticyclonic conditions indicative of clear sky conditions. Data for this fog event were therefore used to carry out simulations in this study.

2.3 Soil moisture data set

The estimation of soil moisture from satellite observations requires ground-based measurements of surface soil moisture content. In New Zealand, such observations are only available from the AWSs operated by Fire and Emergency New Zealand

https://doi.org/10.5194/egusphere-2022-1229
Preprint. Discussion started: 6 December 2022
© Author(s) 2022. CC BY 4.0 License.

(FENZ), and most soil sensors were only deployed at the AWSs in Christchurch after 2018. Consequently, a spatially heterogeneously distributed assessment of soil moisture across Christchurch cannot be derived specifically for the selected case study from 2001. Therefore, in this study, we do not aim to reproduce the soil moisture profiles during the selected radiation fog event. Rather, satellite observations are used as a tool to derive spatial patterns of soil moisture heterogeneity that can be included in the simulations to investigate its impact on the radiation fog life cycle. Based on data availability, Landsat 8 data were used in this study to provide high-resolution soil moisture observations. The moderate resolution imaging spectroradiometer (MODIS) is another potential data source, but MODIS only provides data at resolutions between 250 m and 1 km (Justice et al., 2002). In contrast, Landsat 8 has a spatial resolution of 15 m to 100 m (Roy et al., 2014), and the surface soil moisture heterogeneity can be well-captured with such a high spatial resolution.

Landsat 8 observations from 2nd August 2019 were used to derive the heterogeneously distributed soil moisture profile for this case study, and were obtained from Sentinel Hub EO Browser (Sinergise Ltd, 2022a, b, last access: 14 April 2022). There are several reasons why this day was chosen. First, a winter case was picked so that the soil moisture data represent winter soil conditions over Christchurch. Second, cloud coverage varies with every satellite pass, and for 2nd August 2019 only a few clouds were present when the measurements were made. Therefore, surface soil moisture can be obtained for the entire simulation domain for this day. In addition, no significant precipitation or drought event occurred prior to 2nd August 2019. The derived values of soil moisture fall within the range of long-term measured minimum and maximum values for the Canterbury region, as described in Sohrabinia et al. (2014). This means the derived soil moisture is neither too high nor too low for conducting simulations representing winter conditions. Furthermore, the surface soil moisture values observed by the four FENZ stations (locations shown in Figure 1c) are similar to those obtained from the WRF simulations (not shown), and only minor adjustment is needed to include the derived soil moisture heterogeneity in the PALM simulations.

3 Model and simulation description

3.1 PALM model and simulation configuration

The non-hydrostatic PALM model system 6.0 (r4829) was used to conduct the fog simulations. The PALM simulation configuration is shown in Table 3. Considering the order of magnitude of their sizes, most of the eddies are parameterized in the simulations presented in this study (81 m horizontal grid spacing and 18 m vertical grid spacing). The simulation includes four model domains (Figure 1) using a one-way nesting mode. Figure 2 shows the vertical profiles of the atmosphere and soil used for model initialisation. The vertical profiles of potential temperature (pt), west-east component of wind (u), and south-north component of wind (v) were obtained from the upper air measurements. In addition, data from WRF simulations were used to derive the vertical profiles of water vapour mixing ratio (qv), soil moisture, and soil temperature. These data obtained from WRF are not available from the observational network of Christchurch. The soil moisture and soil temperature profiles were derived from the mean values of the WRF grid points within the PALM simulation domain 4 (D04). The vertical profiles of soil moisture and soil temperature shown in Figures 2e and 2f are used for the homogeneous setup (hereafter HOM), with the values of soil moisture and temperature identical horizontally for each soil layer. To include the spatial heterogeneity of

https://doi.org/10.5194/egusphere-2022-1229
Preprint. Discussion started: 6 December 2022
© Author(s) 2022. CC BY 4.0 License.

Table 3. Configuration of PALM simulation.

Domains	**D01**	**D02**	**D03**	**D04**
Grid spacing west-east (dx)	729 m	729 m	243 m	81 m
Grid points west-east (nx)	144	108	132	216
Grid spacing south-north (dy)	729 m	729 m	243 m	81 m
Grid points south-north (ny)	144	108	96	216
Vertical grid spacing (dz)	162 m	162 m	54 m	18 m
Vertical grid points (nz)	32	18	24	36
Topography	Flat	Derived from DEM	Derived from DEM	Derived from DEM
Radiation model	RRTMG	RRTMG	RRTMG	RRTMG
Land use	short grass	Different types of vegetation, soil, and water bodies, derived from New Zealand LCDB v5.0	Different types of vegetation, soil, and water bodies, derived from New Zealand LCDB v5.0	Different types of vegetation, soil, and water bodies, leaf area density, plant canopy, buildings, streets, and pavements, derived from New Zealand LCDB v5.0 and OpenStreetMap
Bulk cloud model	Off	Off	Off	On (Kessler)
Soil moisture	Homogeneous	Homogeneous	Homogeneous	Heterogeneous
Boundary conditions	Cyclic	Nested	Nested	Nested

soil moisture, a 3D profile of soil moisture (west-east, south-north, and for vertical soil layers) was used at initialisation. For the heterogeneous setup (hereafter HET), the vertical profile of soil moisture was adjusted corresponding to the surface soil moisture heterogeneity derived from Landsat 8. The vertical profiles obtained from the upper air measurements and WRF were processed to create the dynamic driver input files for PALM by using the initialisation profile interpolation functions applied in WRF4PALM (Lin et al., 2021).

https://doi.org/10.5194/egusphere-2022-1229
Preprint. Discussion started: 6 December 2022
© Author(s) 2022. CC BY 4.0 License.

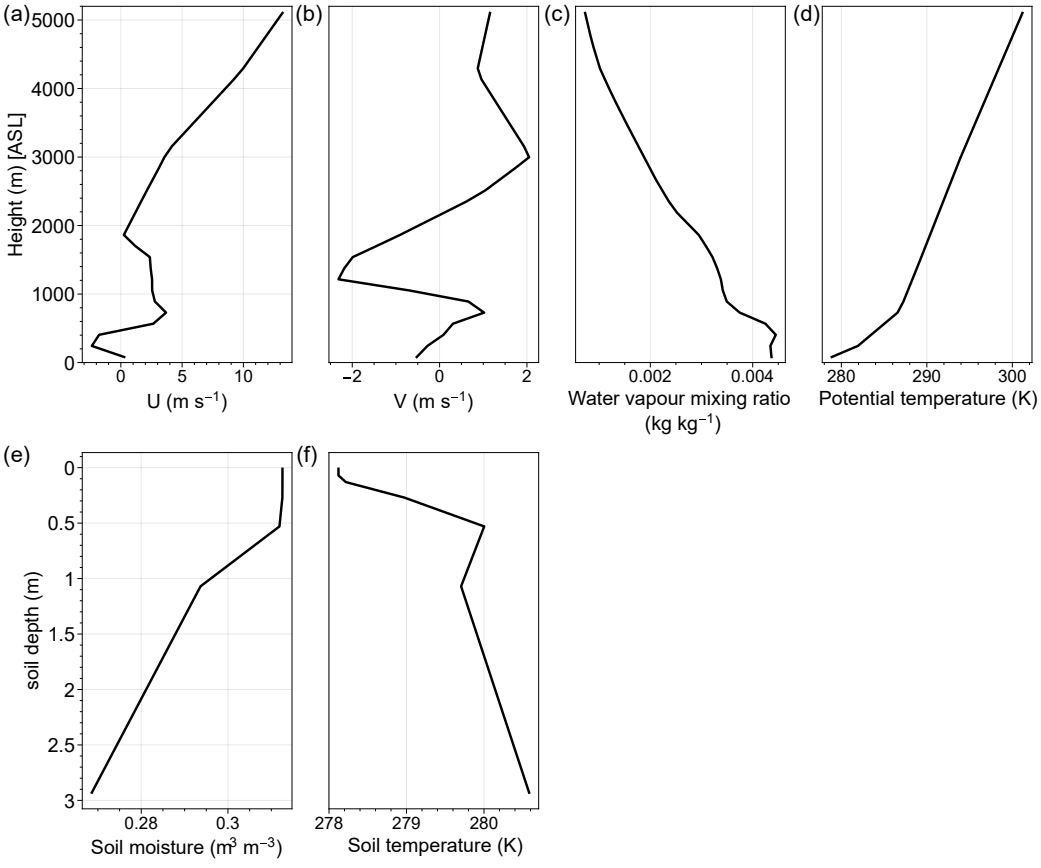

Figure 2. Vertical profiles at simulation initialisation: (a) u wind component, (b) v wind component, (c) water vapour mixing ratio (qv), (d) potential temperature (pt), (e) soil moisture, and (f) soil temperature. Note that the profile of soil moisture shown here was only applied in the simulation with homogeneous soil moisture.

This study does not aim to reproduce the entire radiation fog event accurately. Rather, the aim is to create a radiation fog scenario in a stable boundary layer and use the simulations to provide guidance on the processes involved in the radiation fog life cycle. Therefore, the dynamic driver is only used to initialise the simulations and cyclic lateral boundary conditions are used. All fog simulations in this study have a 48 hour run time and the first 24 hours of the simulations are considered as model spin-up time. Only the second 24 hours of the simulations are therefore included in the analysis. As previously mentioned, the first domain (D01) is configured as flat terrain with the land use type configured as grassland only. This is because grassland is the dominant land use type in the rural area surrounding Christchurch. The purpose of this domain is to pass down the synoptic forcing to the finer domains and maintain a stable boundary layer for fog development. The heterogeneous terrain and land use are enabled for the nested domains to represent the complex rural-urban environment. We focus on D04 to investigate the impact of soil moisture heterogeneity on radiation fog. Therefore, the urban surface model, plant canopy model, and the bulk

https://doi.org/10.5194/egusphere-2022-1229
Preprint. Discussion started: 6 December 2022
© Author(s) 2022. CC BY 4.0 License.

cloud model are only enabled for D04. In domains 2 and 3 (D02 and D03, respectively), different types of vegetation, soil, and water bodies were included (as described in Table 3). Only D04 includes leaf area density, plant canopy, and urban canopy (buildings, pavements, and street).

In the fog simulations, the land surface model (Gehrke et al., 2021), urban surface model (Resler et al., 2017), radiation model (RRTMG) (e.g. Clough et al., 2005), plant canopy model (Maronga et al., 2020), LES-LES nesting, and one-moment bulk cloud model (Kessler, 1969) are used. The bulk cloud model was only applied in D04. Two-moment schemes are not compatible with the plant canopy model of PALM. Fog is identified by converting liquid water mixing ratio (ql) to visibility and when visibility is less than 1 km at any grid points near the surface, fog is recorded. The visibility is calculated as

$$vis = 0.027 \times LWC^{-0.88} \qquad [\mathrm{km}] \tag{1}$$

where LWC is liquid water content (Gultepe et al., 2006) and can be expressed as

$$LWC = ql \times \rho_{air} \qquad [\mathrm{g\ m^{-3}}] \tag{2}$$

where ρ_{air} is air density (Stull, 2017) and the unit of ql is $\mathrm{g\ kg^{-1}}$. Since PALM is an incompressible model, ρ_{air} is considered constant (1.225 $\mathrm{kg\ m^{-3}}$). Although the visibility can also be expressed as an association with cloud droplet number concentration (Gultepe et al., 2006; Schwenkel and Maronga, 2019), cloud droplet number concentration is not included in the one-moment bulk cloud model. For more detailed technical descriptions of PALM, the reader is referred to Maronga et al. (2015), Maronga and Bosveld (2017), and Maronga et al. (2020).

3.2 Soil moisture configuration

This study adopted the soil moisture index calculation method for Landsat 8 imagery described in Avdan and Jovanovska (2016). For our case study, the spatially heterogeneously distributed soil moisture of the simulation domain was first adjusted to have the same mean value as HOM. The soil moisture was then adjusted to amplify the signal of soil moisture heterogeneity. This second adjustment (hereafter readjustment) was designed to amplify the impact of soil moisture heterogeneity on fog development and subsequently to help us understand such impact. Both the aforementioned adjustments were applied to surface soil moisture first. Then, soil moisture at all soil vertical levels was adjusted correspondingly at each grid point such that the slope of the profile did not change.

The readjustment method was applied to an N-by-N readjustment area, where N is a chosen number of grid points, with N applied in both west-east (x) and south-north (y) directions. For each N-by-N readjustment area, the mean soil moisture (SM_{mean}) was calculated. Then, if SM_{mean} was greater than or equal to the soil moisture value for the homogeneous simulation (SM_{HOM}), the soil moisture did not change for the grid points inside the N-by-N readjustment area with soil moisture greater than and equal to SM_{mean}. For grid points inside the N-by-N readjustment area with soil moisture less than SM_{mean}, the soil moisture of the grid points was increased to SM_{mean}. On the other hand, if SM_{mean} was less than SM_{HOM}, the soil moisture value did not change for the grid points inside the N-by-N readjustment area with soil moisture less than SM_{mean}. For grid points inside the N-by-N readjustment area with soil moisture greater than SM_{mean}, the soil moisture of the grid

https://doi.org/10.5194/egusphere-2022-1229
Preprint. Discussion started: 6 December 2022
© Author(s) 2022. CC BY 4.0 License.

points was decreased to SM_{mean}. An example of this soil moisture readjustment is shown in Figure 3. With the readjustment, an N-by-N area with a higher mean value became wetter, while an area with a lower mean value became drier, although the internal heterogeneity of each N-by-N area was preserved.

In this study, the following numbers of west-east and south-north grid points were chosen to apply the readjustment method: 6, 12, 18, 36, 54, and 108 (hereafter denoted as HET6p, HET12p, HET18p, HET36p, HET54p, and HET108p, respectively). These numbers of grid points were chosen as the total number of grid points in each direction (216) for D04 is divisible by them. They also cover the range from microscale to mesoscale (486, 972, 1458, 2916, 4374, and 8748 m). The soil moisture content of the first soil layer of HET (no readjustment applied), and the soil moisture difference between HOM and all the heterogeneous simulations are shown in Figure 4. The soil moisture difference was calculated by subtracting the soil moisture of HOM from that of the heterogeneous simulation. This readjustment method amplifies the dry and wet signal from the original soil moisture heterogeneity while keeping the magnitude of soil moisture changes within a realistic range.

4 Results

4.1 Meteorological controls

In this section, the meteorological controls involved in the simulated radiation fog event are presented and discussed. We only present the results for D04 obtained from HOM as a reference, as the vertical profiles of the atmosphere used for all the simulations are identical. Figure 5 shows the fog duration, qv at fog onset, and the modified Richardson number (MRi) at fog onset at each grid point at the first model level above the surface. The MRi is calculated as:

$$MRi = \frac{T_{air} - T_{sfc}}{u^2} \qquad [\mathrm{K\ m^{-2}\ s^2}] \tag{3}$$

where T_{sfc} is surface temperature, and T_{air} and u are temperature and wind speed at the first model level (9 m above the ground surface), respectively. The MRi was first introduced by Baker et al. (2002) to assess boundary layer turbulence for radiation fog forecasting. The MRi was later adopted by Lin et al. (2022) to classify the fog types in Christchurch. Similar to Lin et al. (2022), here we use MRi to assess the dynamic stability of the near-surface layer. MRi > 0 indicates a stable surface layer with a surface temperature inversion. The more positive the MRi, the stronger the inversion and the smaller the wind speed. MRi < 0 indicates that the surface layer is unstable, with the surface warmer than the overlying air so that turbulence is not suppressed. In general, fog forms at locations with either high positive MRi (strongly stable) or greater qv. This agrees with known characteristics of radiation fog that sufficient radiative cooling and moisture availability play major roles in its formation and development (e.g. Duynkerke, 1991; Gultepe et al., 2007). The small area of fog that occurred to the northwest of the Hagley Park area coincided with greater qv (>0.0054 $\mathrm{kg\ kg^{-1}}$; Figure 5c) at fog onset, but as MRi was negative (as seen in Figure 5d) fog formation was short-lived (less than 1 hour as shown in Figure 5b).

Significant spatial variation of fog occurred in the simulation and several meteorological controls appeared to impact on fog formation, development and dissipation. To provide greater insight into the fog simulation, horizontal cross sections of visibility, qv, and MRi at the first model level for D04 between 1230 UTC and 2030 UTC are shown in Figures 6, 7, and 8.

https://doi.org/10.5194/egusphere-2022-1229
Preprint. Discussion started: 6 December 2022
© Author(s) 2022. CC BY 4.0 License.

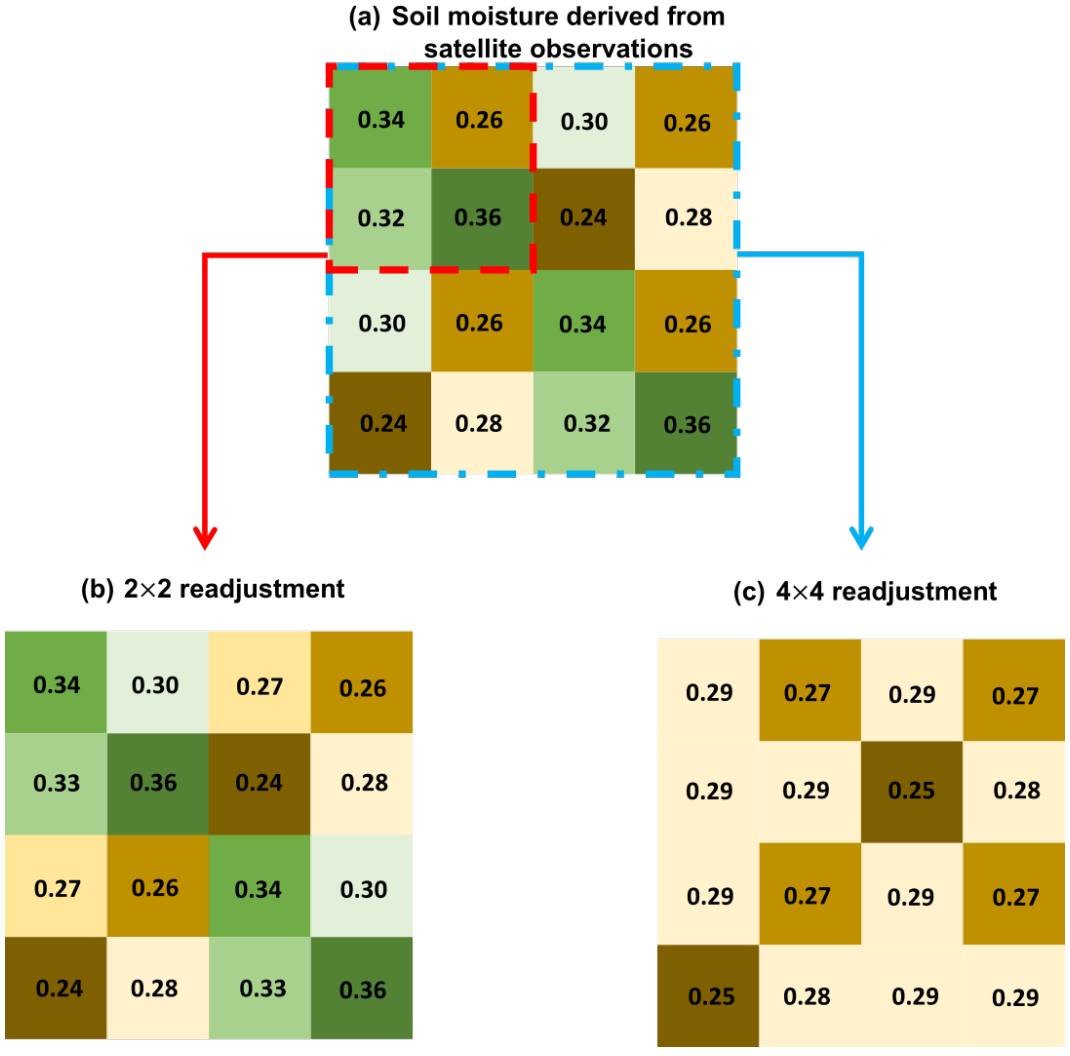

Figure 3. Examples of soil moisture readjustment: (a) demonstrates the soil moisture derived from the satellite observations. The mean value for (a) is 0.295 $\mathrm{m}^3\ \mathrm{m}^{-3}$. Each square box represents one grid point, and the values of each box indicate the soil moisture content in $\mathrm{m}^3\ \mathrm{m}^{-3}$. Boxes in green indicate that the soil moisture of the box is higher than the homogeneous soil moisture value, while boxes in brown indicate lower soil moisture values. (b) shows the results of 2 by 2 readjustment. A 2 by 2 area is highlighted by the red dashed square box in (a). (c) shows the results of 4 by 4 readjustment. A 4 by 4 area is highlighted by the blue dashed dotted square box in (a).

One-hour averages were applied to the horizontal cross sections, and the sunset time for this case study was around 0525 UTC. The white patches around Hagley Park seen in Figure 8 are grid points where vegetation type is deciduous needle leaf trees and the roughness length for heat and momentum is 2 m, which resulted in near zero MRi values. In addition, the one-hour averaged vertical cross sections over central Hagley Park of pt, qv, and ql between 1300 UTC and 1900 UTC are shown in Figure 9. The south-north vertical cross sections were obtained at the 150th grid point along the west-east axis (12190.5 m).

https://doi.org/10.5194/egusphere-2022-1229
Preprint. Discussion started: 6 December 2022
© Author(s) 2022. CC BY 4.0 License.

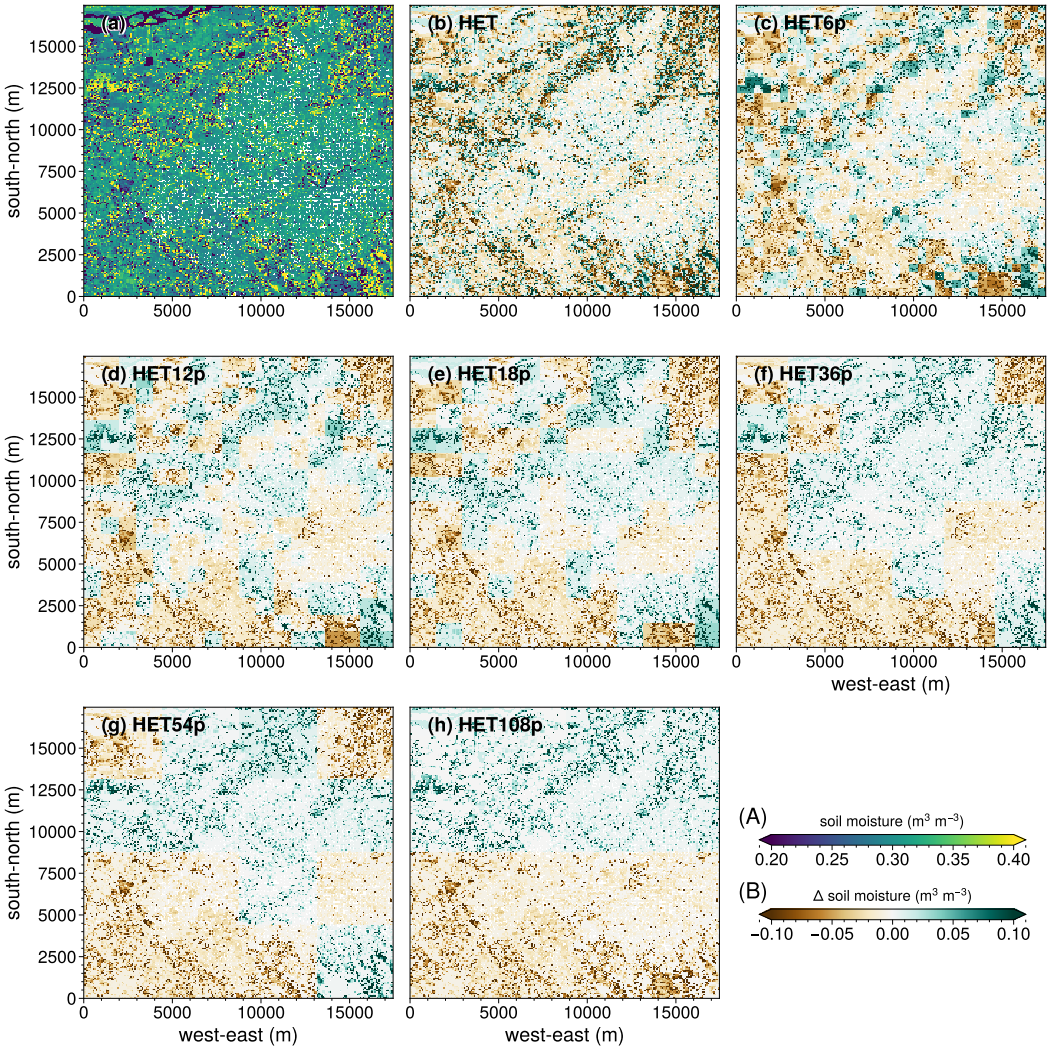

Figure 4. Soil moisture for D04 in HET (a), and soil moisture difference between the heterogeneous simulations and the homogeneous simulation (HOM) for (b) HET, (c) HET6p, (d) HET12p, (e) HET18p, (f) HET36p, (g) HET54p, and (h) HET108p. Colour legend (A) applies to panel (a) only. Colour legend (B) applies to panels (b)-(h). The difference was a result of the soil moisture in the homogeneous simulation subtracted from that of the heterogeneous simulation. Green areas in panels (b)-(h) indicate that soil moisture in the heterogeneous simulation is higher than in HOM, while brown areas indicate drier soil in the heterogeneous simulation.

Fog formation started around the Hagley Park area where the temperature cooled faster than its surroundings (Figures 6a and 9a). The Hagley Park area is located in the low-lying centre of the city (at about 9 m above mean sea level) with the Canterbury Plains rising to the west (Christchurch airport at 35 m above mean sea level) and the Port Hills to the south (at about 400 m above mean sea level) (Figure 1c). During the entire simulation period, the surface wind speed over this area did not exceed 1.5 $\mathrm{m\ s^{-1}}$, remaining well below 0.5 $\mathrm{m\ s^{-1}}$ during night time. The low wind speed enhances the sheltering effect, and the flow

https://doi.org/10.5194/egusphere-2022-1229
Preprint. Discussion started: 6 December 2022
© Author(s) 2022. CC BY 4.0 License.

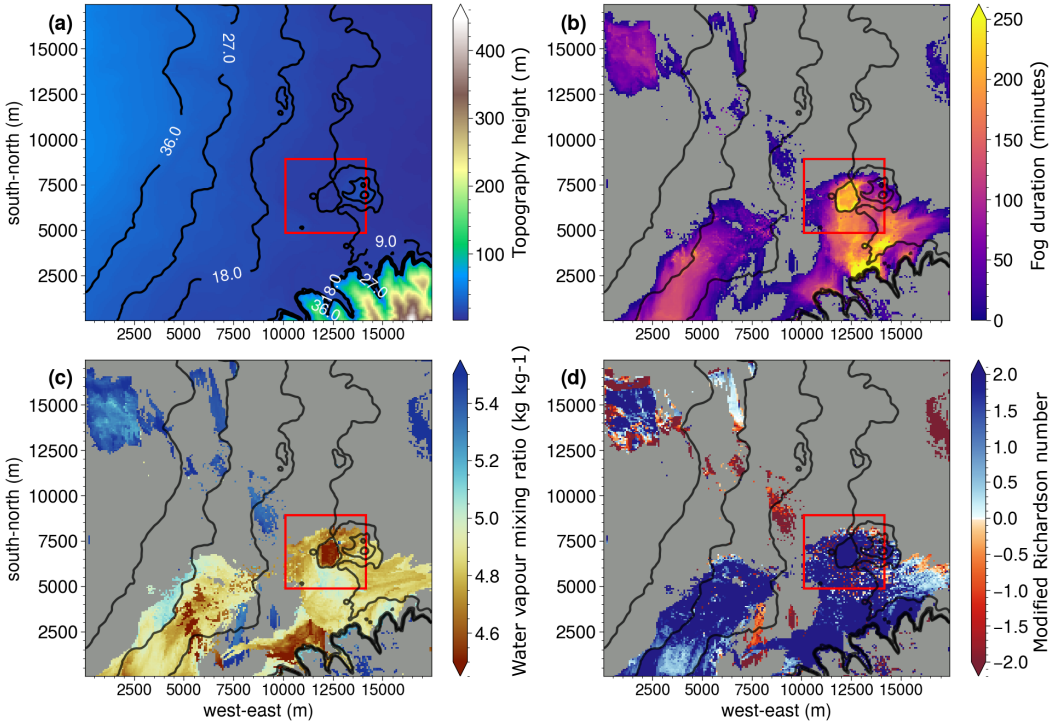

Figure 5. (a) Topographic map of D04 with black contour lines indicating terrain height between 9 m and 36 m. Panels (b), (c), and (d) are fog duration in minutes, water vapour mixing ratio (qv) at fog formation, and the modified Richardson number (MRi) at fog formation at the first model level for D04, respectively. Contour lines in panels (b), (c), and (d) indicate terrain height labelled in panel (a). Grey areas in (b), (c), and (d) are where no fog occurred. The location of Hagley Park is indicated by a red box in each panel.

within the Hagley Park area would have become decoupled from the flow outside. A stable layer therefore started to form with reduced downward turbulent heat flux. The stable near-surface layer over Hagley Park is highlighted by the high positive MRi shown in Figures 8a-c. While the stable layer and fog were developing, the northwesterly flow coming across the Canterbury Plains from the foothills of the Southern Alps and the southeasterly flow coming from the Port Hills were converging across Christchurch. The convergence zone is visible in the wind vector fields shown in Figures 6a-c, which agrees with the wind field described in Corsmeier et al. (2006). During the entire simulation, fog rarely formed over the northern half of the D04 domain, and as shown in Figures 8a-c, the MRi values were near-zero or negative over this area. This is due to clouds that formed over this area at around 400 m above the ground, while the southern part of the simulation domain was under clear sky (see Figure 9i). The formation of clouds is considered to result from high qv at around 400 m at model initialisation (Figure 2c), with high values of qv at approximately 400 m also visible in Figures 9e-h. The cloud layer led to more incoming longwave radiation to the surface over the northern section of D04, which might have led to a decrease of surface cooling and subsequently a less stable layer over this area. Although the northerly flow was associated with generally higher qv at around 1830 UTC (Figure 7g-i), fog did not form or only developed for a very short period of time over the north of D04 (Figures 6g-i). One explanation

https://doi.org/10.5194/egusphere-2022-1229
Preprint. Discussion started: 6 December 2022
© Author(s) 2022. CC BY 4.0 License.

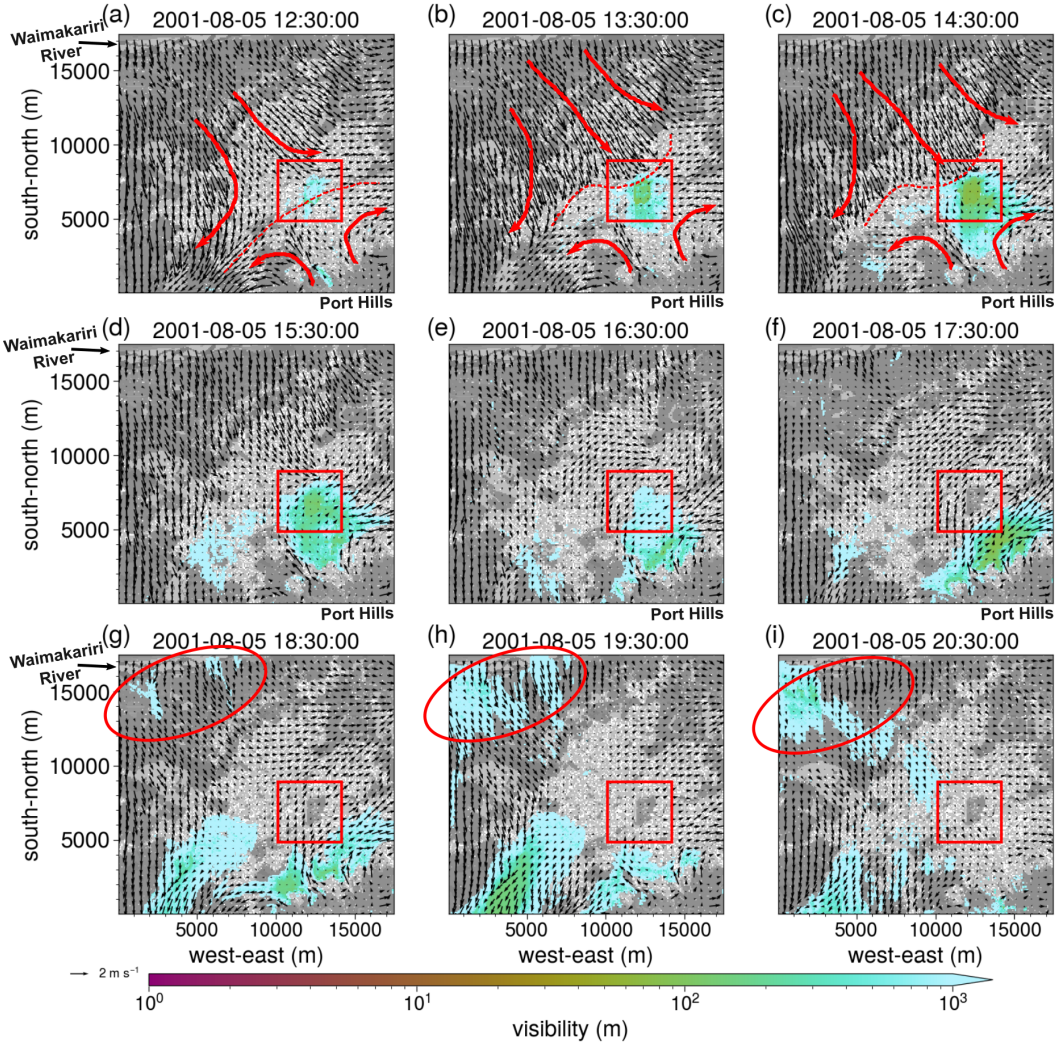

Figure 6. Visibility and wind vectors at the first model level between 1230 UTC and 2030 UTC on 5th August 2001. The background image shows the land use over D04 - white patches represent buildings and dark grey areas are vegetated or water bodies. An interpretation of the drainage flow (solid red arrows) and the convergence zone (dashed red lines) is shown in panels (a)-(c). The location of Hagley Park is indicated by a red box in each panel. The Waimakariri River and Port Hills are located in the northwest and the southeast of D04, respectively. The red ellipses indicate where fog is related to the Waimakariri River.

295 is that when qv increased to over 0.0052 $\mathrm{kg\ kg^{-1}}$ over the northwest (Figures 7h-i), it was around sunrise time (1936 UTC) when the clouds over the north and fog over the south started to lift and dissipate.

Between 1300 UTC and 1500 UTC, as the stable layer developed further around Hagley Park, fog started to form and develop in the surrounding areas (Figures 6a-d). Since the northern part of D04 remained less stable, the northwesterly flow was relatively strong (1.5 $\mathrm{m\ s^{-1}}$) during this period. This flow lifted above the cold air drainage from the Port Hills, the stable

https://doi.org/10.5194/egusphere-2022-1229
Preprint. Discussion started: 6 December 2022
© Author(s) 2022. CC BY 4.0 License.

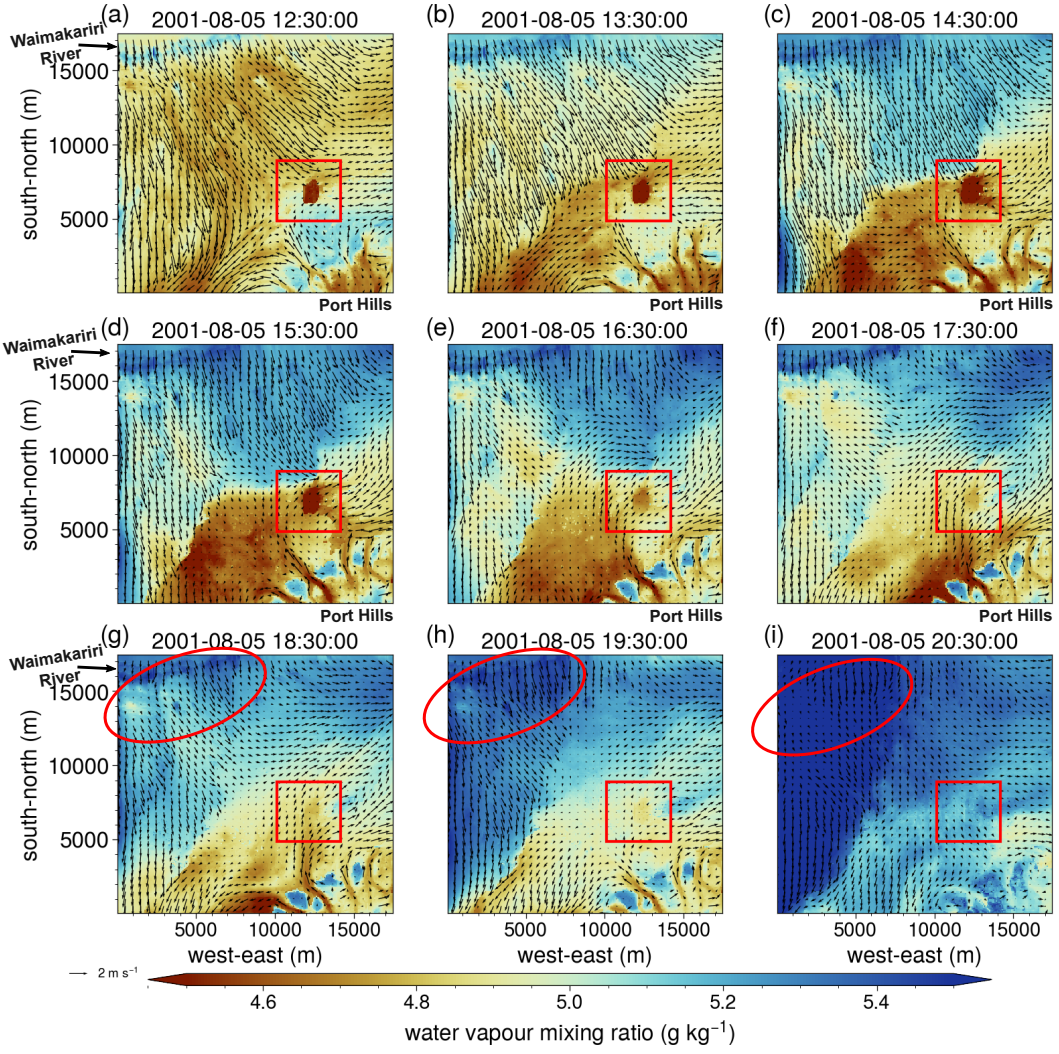

Figure 7. Similar to Figure 6, but for water vapour mixing ratio (qv) and wind vectors.

layer, and the fog top over Hagley Park (Figure 9j), thereby controlling the fog thickness. Consequently, the fog layer over Hagley Park was unable to develop above approximately 100 m. The interaction between the relatively strong northerly flow and the fog top is considered to be an important factor leading to fog dissipation over Hagley Park. Vertical entrainment appears to have resulted in turbulent mixing at the fog top over this area, while the northerly flow pushed the convergence zone to the south. As a result, fog dissipated over Hagley Park and its surrounding areas and started to retreat to the south along the base of Port Hills (Figure 6d-g). The fog kept developing in pockets along the edge of the Port Hills where the surface layer was highly stable in association with high water vapour mixing ratio near the surface (Figures 6e-g, 7e-g, and 8e-g). The fog was not sustained over the valleys (refer to Figure 9a for topography height) where the flows were channelled down from the Port Hills.

https://doi.org/10.5194/egusphere-2022-1229
Preprint. Discussion started: 6 December 2022
© Author(s) 2022. CC BY 4.0 License.

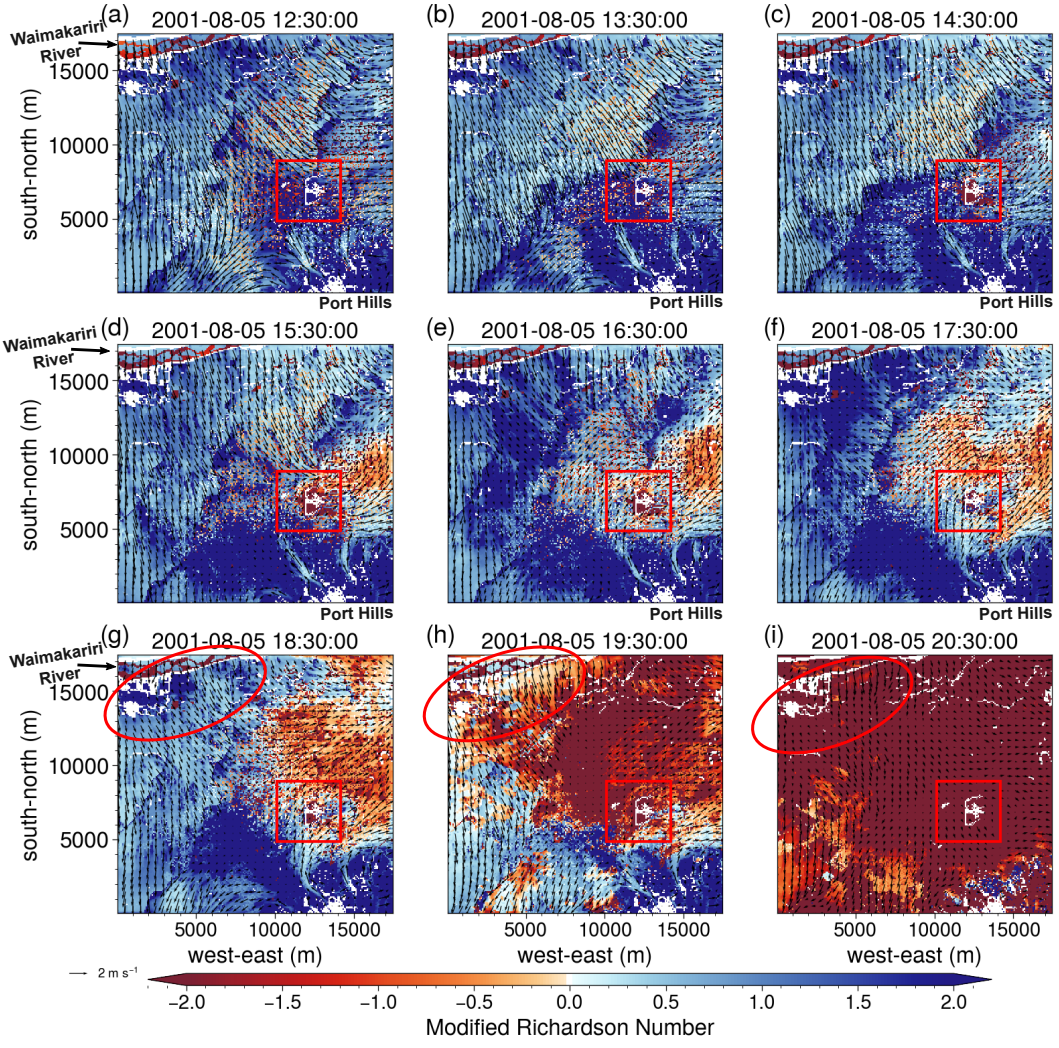

Figure 8. Similar to Figure 6, but for the modified Richardson number (MRi) and wind vectors. White patches are either water bodies or vegetation with a roughness length of 2 m for momentum and heat.

At around 1830 UTC, the southeasterly flow from the Port Hills converged with the northerly flow over the central southern section of D04, where another stable layer developed and fog started to form. The fog was later advected to the southwest of D04 by the converged flow turning to become northeasterly. In addition, one can notice that another fog event occurred over the northwest corner of D04 (Figures 6h-i; red circled area), forming at around 1900 UTC. This was considered to be a result of water vapour evaporating from the Waimakariri River located to the northwest of Christchurch and condensing into liquid water. High qv was presented over the Waimakariri River throughout the entire period as shown in Figure 7. The duration of these two fog events later in the morning was relatively short as they both occurred near sunrise and dissipated soon after due

https://doi.org/10.5194/egusphere-2022-1229
Preprint. Discussion started: 6 December 2022
© Author(s) 2022. CC BY 4.0 License.

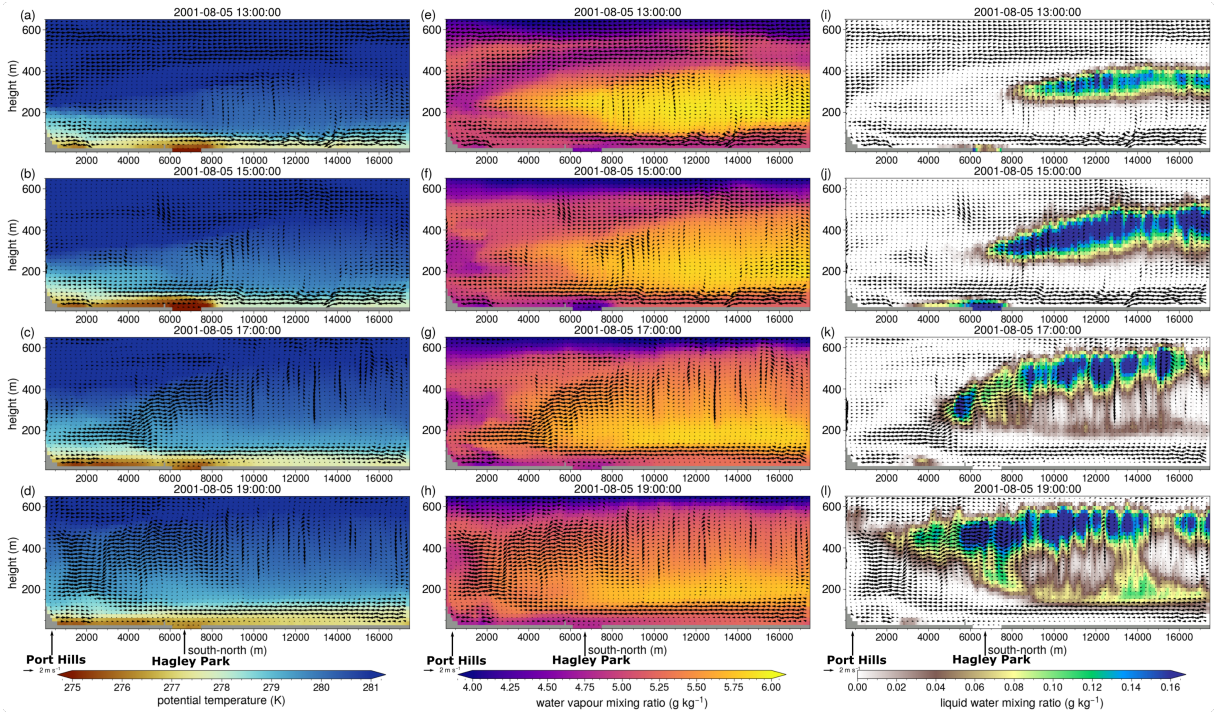

Figure 9. South-north vertical cross sections over central Hagley Park (west-east distance at 12190.5 m) of wind vectors (v), potential temperature (pt) (a-d), water vapour mixing ratio (qv) (e-h), and liquid water mixing ratio (ql) (i-l). Grey areas indicate topography.

315 to an increase in incoming shortwave radiation and turbulent mixing. In the meantime, the stable near-surface layer over the entire domain decayed and became unstable (Figures 8g-i).

4.2 Fog sensitivity to soil moisture heterogeneity

In the environment of heterogeneous topography and soil moisture, the simulated formation and dissipation times of fog at each grid point are different in each simulation. Therefore, we focus on fog duration to assess the sensitivity of fog to
320 changes in soil moisture heterogeneity. Fog duration at the first model level was calculated for all the eight simulations and the results are compared in Figure 10. The comparison shows significant spatial variation in fog duration between HOM and each heterogeneous simulation. However, the strong topographical and meteorological steering restricts deviations in the simulated locations of fog occurrence under this typical meteorological scenario. In this particular fog case study, the amplified soil moisture heterogeneity does not significantly alter the fog occurrence patterns (Figure 10). Nevertheless, fog duration shows
325 high sensitivity to soil moisture heterogeneity and the resulting changes in fog duration can be more than 50 minutes for some areas (Figures 10b-h). However, there is no direct evidence to link the changes in soil moisture to the changes in fog duration. When compared at each grid point, the changes in fog duration shown in Figure 10 do not mirror the changes in soil moisture shown in Figure 4. For example, HET and HET108p have significantly different soil moisture patterns (Figures 4b

https://doi.org/10.5194/egusphere-2022-1229
Preprint. Discussion started: 6 December 2022
© Author(s) 2022. CC BY 4.0 License.

and 4h), while the decrease or increase in fog duration (Figures 10b and 10h) does not show considerable variation between the two simulations. Both HET12p and HET18p show areas of increase in fog duration near the Port Hills in the southeast of D04 (Figures 10d and 10e), while this pattern is absent in other heterogeneous simulations. The HET simulation results in a decrease in fog duration over the southwest part of D04 (blue box in Figure 10b), while HET6p and HE12p show an increase in fog duration in this area (blue boxes in Figures 10c and 10d). This pattern was not present in HET18p and HET36p (blue boxes in Figures 10e and 10f), where the heterogeneous signals were further amplified.

Maronga and Bosveld (2017) investigated the sensitivity of radiation fog to the initial state of soil temperature and humidity. Their results suggest that changes in soil moisture content do not affect fog formation time, although fog lifting time is affected. Our simulations do not agree with their findings, as both the formation and dissipation times vary in each simulation (not shown). As both Maronga and Bosveld (2017) and our study used PALM, we believe the difference in the results is due to a different simulation setup. For example, spin-up time for Maronga and Bosveld (2017) was only 35 minutes, while our spin-up time was 24 hours, so that daytime evaporation from the soil is not included in their simulations. The fog lifting and dissipation period in Maronga and Bosveld (2017) occurred during sunrise, while fog dissipation time in our study varied across the simulation domain. Maronga and Bosveld (2017) simulated their radiation fog event over flat terrain with land use type configured as grassland only and did not include spatial heterogeneity in soil moisture. In addition, the range of soil moisture heterogeneity values in our study is smaller than Maronga and Bosveld (2017). Their simulations used soil moisture at wilting point and at saturation across a range of values greater than 0.15 $\mathrm{m}^3\ \mathrm{m}^{-3}$, while as shown in Figure 4, over 70% of the grid points in our study are associated with a a range of values less than 0.05 $\mathrm{m}^3\ \mathrm{m}^{-3}$. It should be noted that this value falls within a typical range of soil moisture values over a diurnal cycle (between -0.1 $\mathrm{m}^3\ \mathrm{m}^{-3}$ and 0.1 $\mathrm{m}^3\ \mathrm{m}^{-3}$; Meng and Quiring, 2008). Furthermore, the mean values of soil moisture for D04 for all simulations are identical. This highlights the importance of including soil moisture heterogeneity in fog forecasting, as fog duration can be very sensitive to small changes in soil moisture and soil moisture heterogeneity.

5 Conclusions, discussion, and outlook

A set of numerical fog simulations was conducted to investigate the impacts of meteorological controls on radiation fog in Christchurch using the microscale model PALM. As Christchurch's observational network does not have a great spatial and vertical coverage, we did not attempt to replicate a real radiation fog event in our simulations. Rather, we conducted simulations using profiles from a selected radiation fog event to create a radiation fog scenario as guidance for future fog research and forecasting. We aimed to understand the impact of soil moisture heterogeneity on fog development, with our case study showing that both mesoscale and microscale dynamics are important. The meteorological controls in a heterogeneous environment were illustrated. To the best of our knowledge, this study is the first to include heterogeneous topography, land use, and soil moisture in radiation fog simulation at the microscale.

Overall, the macrostructure of fog occurrence and distribution is highly controlled by topography and the mesoscale meteorology, while fog duration is sensitive to changes in soil moisture heterogeneity at microscale. As illustrated in Section 3,

https://doi.org/10.5194/egusphere-2022-1229
Preprint. Discussion started: 6 December 2022
© Author(s) 2022. CC BY 4.0 License.

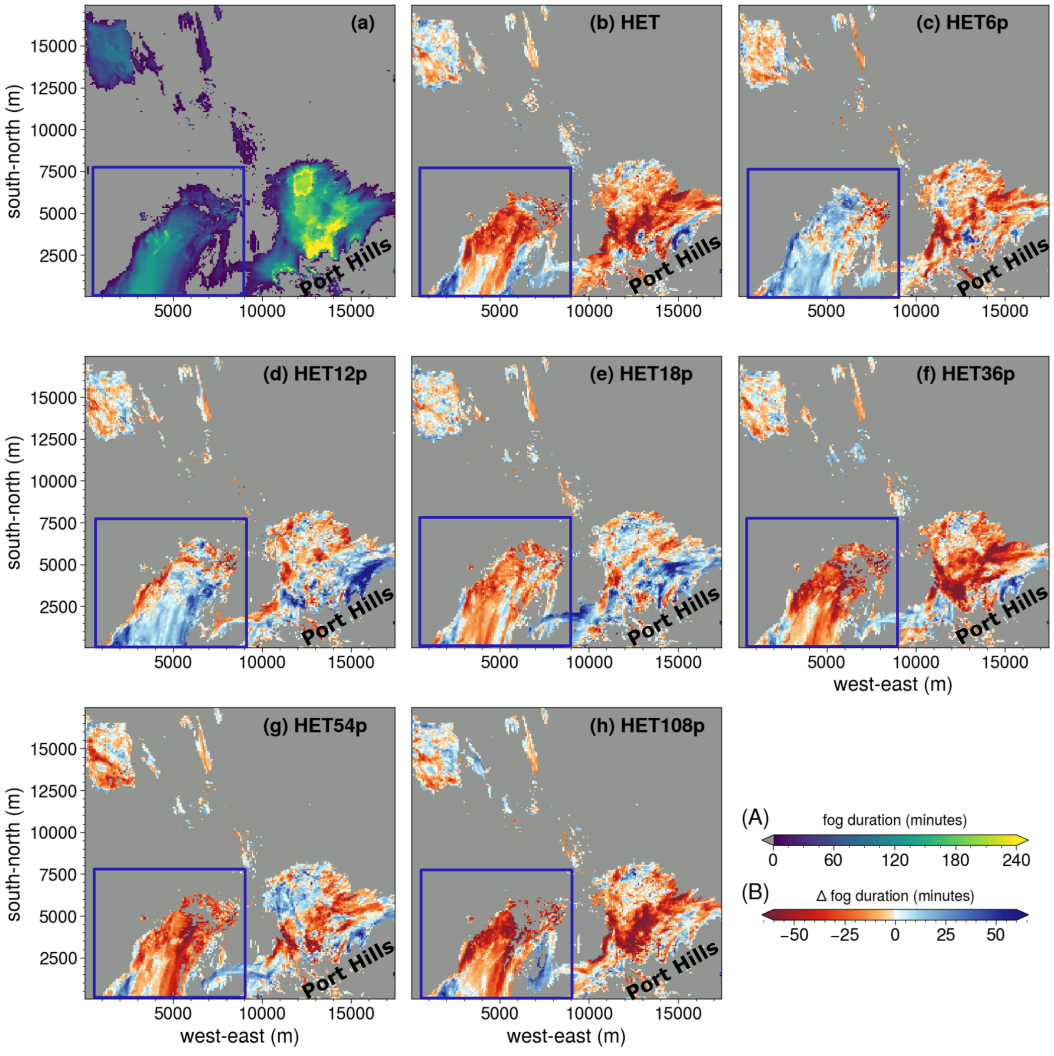

Figure 10. (a) Total fog duration in minutes at the first level above the surface for HOM. Grey areas are where fog did not occur. Panels (b)-(h) show fog duration difference between the heterogeneous simulations and HOM for HET, HET6p, HET12p, HET18p, HET36p, HET54p, and HET108p, respectively. The fog duration difference is the result of the heterogeneous simulations subtracted from HOM. Grey areas in panels (b)-(h) are where fog did not occur in both HOM and the corresponding heterogeneous simulation. Colour legend (A) applies to panel (a) only. Colour legend (B) applies to panels (b)-(f). The blue box in each panel indicates the location of the fog event in the southwest part of D04.

the synoptic situation, drainage flow, local topography, cloud layer, and local radiative cooling all affect the onset, duration, dissipation and spatial distribution of radiation fog. At microscale, the readjustment of soil moisture heterogeneity does not alter the general near-surface wind flow structure and the location of fog occurrence in the simulations. While the range of soil moisture heterogeneity values applied in this case study is relatively small, all the seven heterogeneous simulations resulted in

https://doi.org/10.5194/egusphere-2022-1229
Preprint. Discussion started: 6 December 2022
© Author(s) 2022. CC BY 4.0 License.

significant variations of fog duration. For some areas, when compared to the homogeneous setting, the fog duration can vary by more than 50 minutes, which could be significant for aviation forecasts. The spatial variation in fog duration, however, does not mirror the spatial heterogeneity in soil moisture. Variations in soil moisture may contribute to changes in fog formation and dissipation in several ways. For instance, evaporation from wet soil during daytime is assumed to be a potential source of water vapour in the atmosphere. As highlighted by Maronga and Bosveld (2017), drier soil is associated with faster heating after sunrise and subsequently can lead to earlier fog dissipation. However, with the inclusion of heterogeneous topography, land use, and soil moisture, the present simulations demonstrate significant complexity. Spatial analysis is difficult within such a heterogeneous environment, and it was not possible to identify and analyse the contribution of microscale soil moisture heterogeneity to changes in fog duration. Multiple meteorological controls can modify the local airflow structure and consequently the spatial structure and duration of fog. The contribution of soil moisture heterogeneity appears to be less significant than suggested by previous studies, in which complex topography and/or land surface characteristics were not represented. Nevertheless, our study highlighted that soil moisture heterogeneity can lead to changes in radiation fog duration.

More work is required to further identify and understand the impact of soil moisture heterogeneity on radiation fog, such as through further case studies as we present only one case study here. Lack of observational data is one of the biggest challenges; more observational data from, for example, field campaigns, are necessary to advance fog research. Development of an accurate soil moisture observation network may be necessary, in order to apply heterogeneous soil moisture derived from satellite observations for operational fog forecasts. The soil moisture values were only used in this study to investigate the impact of soil moisture heterogeneity on radiation fog and do not represent the true soil moisture for a real case. Due to the difficulty in spatial analysis and the significant computational cost, we only carried out simulations at a horizontal grid spacing of 81 m. With PALM's high scalability at microscale, the grid spacing of the simulations could be finer so that the turbulence structures can be better resolved and captured. One possible way to further identify the impact of soil moisture heterogeneity is using a Lagrangian method to identify the sources of heat and water vapour. For example, a Lagrangian method was applied by Dale et al. (2020) to identify heat sources near the Ross Sea Polynya.

Only cyclic boundary conditions were used in our simulations. Future fog studies should consider using non-cyclic boundary conditions from NWP models to conduct more realistic fog simulations. This can be achieved using the offline nesting feature embedded in PALM using tools such as WRF4PALM (Lin et al., 2021) and INIFOR (Kadasch et al., 2021). In addition, idealised simulations similar to those configured in Maronga and Bosveld (2017) should be carried out along with observational data to provide greater insight into the impact of soil moisture heterogeneity on fog development and to support the findings of this study.

Code availability. This study used the free and open-source WRF model system V4.2 and the WRF Preprocessing System (WPS) V4.2 (download is available at https://github.com/wrf-model/WRF/releases, last access: 26 October 2022). The PALM model system 6.0 used in this study is a free and open-source numerical atmospheric model. PALM source code is available online (http://palm-model.org, last

https://doi.org/10.5194/egusphere-2022-1229
Preprint. Discussion started: 6 December 2022
© Author(s) 2022. CC BY 4.0 License.

access: 26 October 2022) under the GNU General Public License v3. The exact PALM model source code (revision 4829) is available at https://palm.muk.uni-hannover.de/trac/browser? rev=4829 (last access: 26 October 2022).

Data availability. All PALM input files for the heterogeneous case described in Section 3, including the RRTMG input files, the static driver, the dynamic driver, and its configuration file for all the simulation domains, are available in the Supplement.

Appendix A: Fog event observations and synoptic conditions

The time series of the AWS and sodar observations for the selected fog event are shown in Figure A1. This radiation fog event occurred during the sodar operational period in the winter of 2001. The first order difference of the vertical profiles of the sodar backscatter is derived along the height axis to highlight the elevation of the temperature inversion (Figure A1a). The high values indicate where the backscatter signal is the strongest, which is where the inversion occurred. Some strong signals at the lowest levels (approximately 10 m) are due to ground clutter. At around 1000 UTC on 5th August, the inversion started to develop at around 50 m. The inversion further developed to around 120 m by 1700 UTC 5th August and visibility decreased to below 1000 m. The inversion was sustained over the next 10 hours and the visibility only increased to above 1000 m after 0000 UTC 6th August. The AWS observations at 10 m above ground show westerly and north-westerly winds near the surface before the fog formed, indicating that the air mass was moving down the Canterbury Plains towards the coast, while the sodar observations show northerly and easterly at 30 m. The surface wind speed was below 1.5 $\mathrm{m\ s^{-1}}$ between 0600 UTC 5th August and 0100 UTC 6th August, while the wind speed at 30 m was stronger, but in general below 3.5 m $\mathrm{s^{-1}}$. Significant cooling was recorded between 0600 UTC and 1300 UTC on 5th August (from approximately 7 °C to –1 °C), and relative humidity was above 97%. Observations from the AWS show that the cloud height was above 7500 m before fog onset, but no cloud base lowering was recorded. The cloud base was low after 0100 UTC 6th August because the fog layer developed into mist and the mist layer was observed as a cloud layer.

The synoptic conditions between 0600 UTC 5th August and 0000 UTC 6th August are shown in Figure A2. An anticyclone was centred to the northeast of New Zealand with a ridge extending to the southwest. The location of the ridge over the South Island indicates less cloudy conditions. No significant precipitation was recorded within 5 days before the fog event (not shown) so that the state of soil moisture was not particularly high. Based on the evidence and the available data, this fog event was considered suitable to conduct radiation fog simulations to investigate our research questions.

https://doi.org/10.5194/egusphere-2022-1229
Preprint. Discussion started: 6 December 2022
© Author(s) 2022. CC BY 4.0 License.

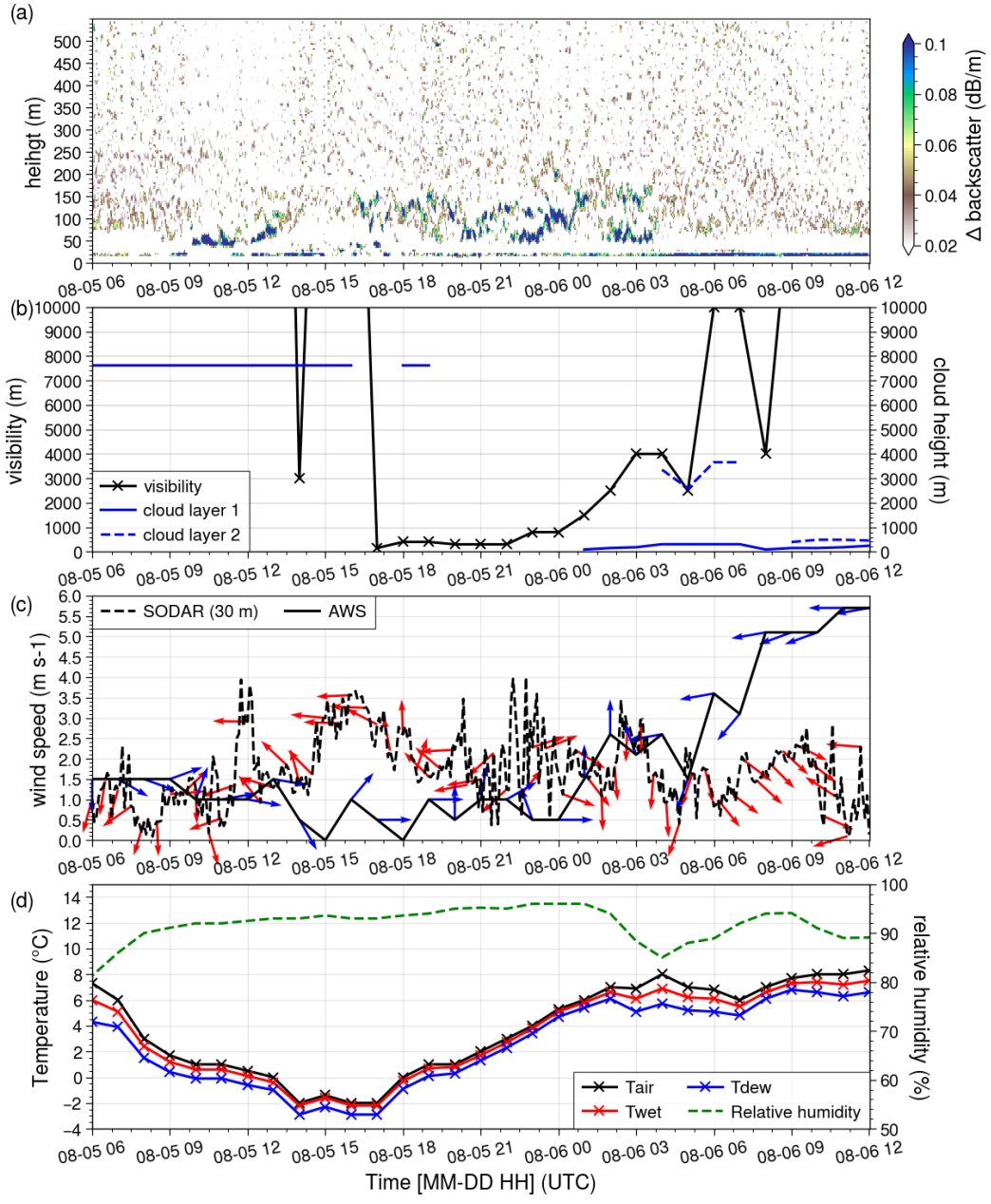

Figure A1. (a) Vertical time section of sodar backscatter, (b) time series of observed visibility and cloud height, (c) wind speed and direction taken from the AWS (10 m) at CHA and from a height of 30 m from sodar observations, (d) air temperature (T_{air}), wet bulb temperature (T_{wet}), dew point temperature (T_{dew}), and relative humidity from the AWS at CHA.

https://doi.org/10.5194/egusphere-2022-1229
Preprint. Discussion started: 6 December 2022
© Author(s) 2022. CC BY 4.0 License.

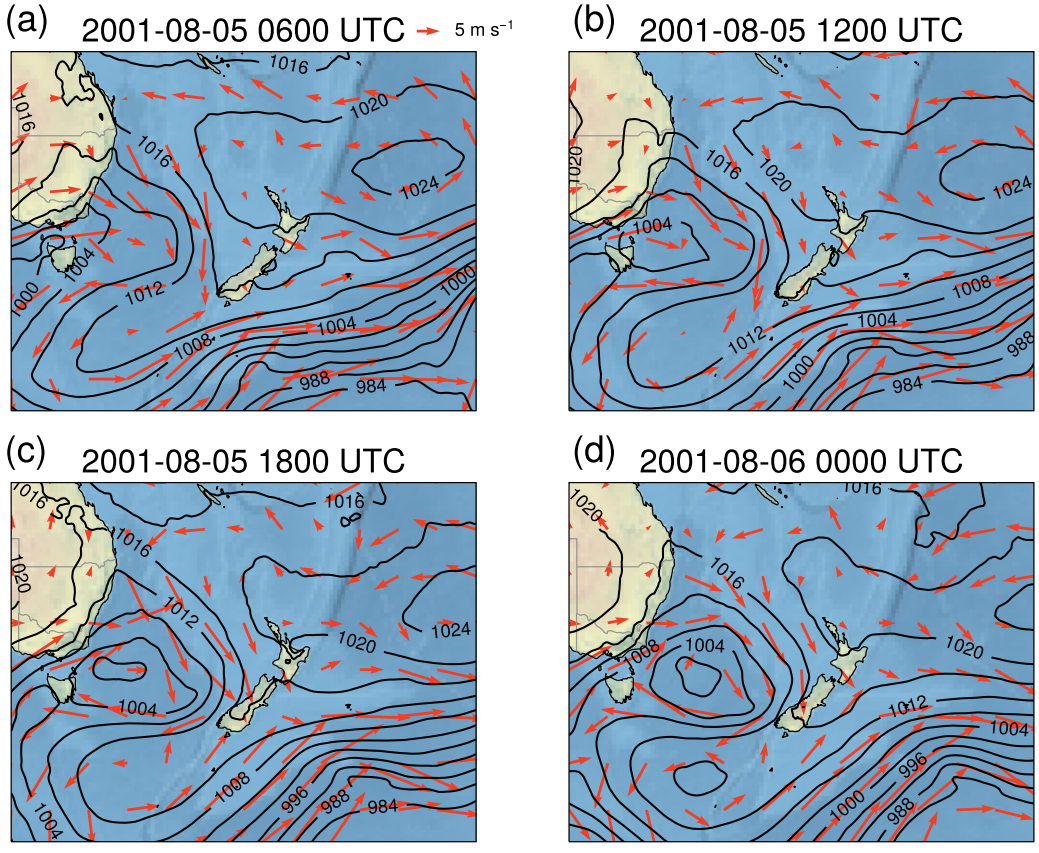

Figure A2. Mean sea level pressure (hPa) and 10 m wind vectors at (a) 0600 UTC, (b) 1200UTC, and (c) 1800 UTC on 5 August 2001 and at (d) 0000 UTC on 6 August 2001. Data were obtained from ERA5 (Hersbach et al., 2019).

https://doi.org/10.5194/egusphere-2022-1229
Preprint. Discussion started: 6 December 2022
© Author(s) 2022. CC BY 4.0 License.

Author contributions. AS provided sodar data for analysis. DL was responsible for the data aquasition, setting and running WRF and PALM simulations, and analysed the results. MK, LER, and BK supervised DL in designing and performing the case studies. DL wrote the manuscript with contributions from MK, LER, BK, and AS. DL, MK, LER, BK, and AS reviewed the manuscript.

Competing interests. The authors declare that they have no conflict of interest.

Acknowledgements. We would like to acknowledge New Zealand eScience Infrastructure (NeSI) high-performance computing facilities for providing computation resources for performing PALM simulations. We would like to thank Françios Bissey and the University of Canterbury high-performance computing cluster for providing computation resources for WRF simulations. The contribution of Dongqi Lin and Laura E. Revell was supported by the University of Canterbury and the Ministry of Business, Innovation and Employment project Particulate Matter Emissions Maps for Cities (grant no. BSCIF1802). Basit Khan received support from the MOSAIK and MOSAIK-2 projects, which are funded by the German Federal Ministry of Education and Research (BMBF) (grant nos. 01LP1601A and 01LP1911H), within the framework of Research for Sustainable Development (FONA; http://www.fona.de, last access: 26 October 2022). Marwan Katurji received support from the Royal Society of New Zealand (contract no. RDF-UOC1701).

https://doi.org/10.5194/egusphere-2022-1229
Preprint. Discussion started: 6 December 2022
© Author(s) 2022. CC BY 4.0 License.

References

Avdan, U. and Jovanovska, G.: Algorithm for automated mapping of land surface temperature using LANDSAT 8 satellite data, Journal of sensors, 2016, 2016.

Baker, R., Cramer, J., and Peters, J.: Radiation fog: UPS Airlines conceptual models and forecast methods, in: Proc. 10th Conf. on Aviation, Range and Aerospace Meteorology, pp. 154–159, 2002.

Bari, D., Bergot, T., and El Khlifi, M.: Local meteorological and large-scale weather characteristics of fog over the Grand Casablanca region, Morocco, Journal of Applied Meteorology and Climatology, 55, 1731–1745, 2016.

Belorid, M., Lee, C. B., Kim, J.-C., and Cheon, T.-H.: Distribution and long-term trends in various fog types over South Korea, Theoretical and Applied Climatology, 122, 699–710, https://doi.org/10.1007/s00704-014-1321-x, 2015.

Bergot, T. and Lestringant, R.: On the predictability of radiation fog formation in a mesoscale model: a case study in heterogeneous terrain, Atmosphere, 10, 165, 2019.

Bergot, T., Escobar, J., and Masson, V.: Effect of small-scale surface heterogeneities and buildings on radiation fog: Large-eddy simulation study at Paris-Charles de Gaulle airport, Quarterly Journal of the Royal Meteorological Society, 141, 285–298, https://doi.org/10.1002/qj.2358, 2015.

Bou-Zeid, E., Meneveau, C., and Parlange, M. B.: Large-eddy simulation of neutral atmospheric boundary layer flow over heterogeneous surfaces: Blending height and effective surface roughness, Water Resources Research, 40, 2004.

Brown, R. and Roach, W. T.: The physics of radiation fog: II–a numerical study, Quarterly Journal of the Royal Meteorological Society, 102, 335–354, iSBN: 0035-9009 Publisher: Wiley Online Library, 1976.

Clough, S. A., Shephard, M. W., Mlawer, E. J., Delamere, J. S., Iacono, M. J., Cady-Pereira, K., Boukabara, S., and Brown, P. D.: Atmospheric radiative transfer modeling: a summary of the AER codes, Journal of Quantitative Spectroscopy and Radiative Transfer, 91, 233–244, https://doi.org/10.1016/j.jqsrt.2004.05.058, 2005.

Corsmeier, U., Kossmann, M., Kalthoff, N., and Sturman, A.: Temporal evolution of winter smog within a nocturnal boundary layer at Christchurch, New Zealand, Meteorology and Atmospheric Physics, 91, 129–148, 2006.

Courault, D., Drobinski, P., Brunet, Y., Lacarrere, P., and Talbot, C.: Impact of surface heterogeneity on a buoyancy-driven convective boundary layer in light winds, Boundary-layer meteorology, 124, 383–403, iSBN: 1573-1472 Publisher: Springer, 2007.

Cuxart, J.: When Can a High-Resolution Simulation Over Complex Terrain be Called LES?, Frontiers in Earth Science, 3, 2015.

Dale, E. R., Katurji, M., McDonald, A. J., Voss, P., Rack, W., and Seto, D.: A comparison of AMPS forecasts near the Ross Sea polynya with Controlled Meteorological balloon observations, Journal of Geophysical Research: Atmospheres, 125, e2019JD030 591, 2020.

Ducongé, L., Lac, C., Vié, B., Bergot, T., and Price, J. D.: Fog in heterogeneous environments: the relative importance of local and non-local processes on radiative-advective fog formation, Quarterly Journal of the Royal Meteorological Society, 146, 2522–2546, https://doi.org/10.1002/qj.3783, 2020.

Duynkerke, P. G.: Radiation Fog: A Comparison of Model Simulation with Detailed Observations, Monthly Weather Review, 119, 324–341, https://doi.org/10.1175/1520-0493(1991)119<0324:RFACOM>2.0.CO;2, publisher: American Meteorological Society Section: Monthly Weather Review, 1991.

Environment Canterbury Regional Council: Christchurch and Ashley River, Canterbury, New Zealand 2018, https://doi.org/https://doi.org/10.5069/G91J97WQ, 2020.

https://doi.org/10.5194/egusphere-2022-1229
Preprint. Discussion started: 6 December 2022
© Author(s) 2022. CC BY 4.0 License.

Gehrke, K. F., Sühring, M., and Maronga, B.: Modeling of land–surface interactions in the PALM model system 6.0: land surface model description, first evaluation, and sensitivity to model parameters, Geoscientific Model Development, 14, 5307–5329, https://doi.org/10.5194/gmd-14-5307-2021, publisher: Copernicus GmbH, 2021.

Gultepe, I., Müller, M. D., and Boybeyi, Z.: A new visibility parameterization for warm-fog applications in numerical weather prediction models, Journal of Applied Meteorology and Climatology, 45, 1469–1480, 2006.

Gultepe, I., Tardif, R., Michaelides, S. C., Cermak, J., Bott, A., Bendix, J., Müller, M. D., Pagowski, M., Hansen, B., Ellrod, G., Jacobs, W., Toth, G., and Cober, S. G.: Fog Research: A Review of Past Achievements and Future Perspectives, Pure and Applied Geophysics, 164, 1121–1159, https://doi.org/10.1007/s00024-007-0211-x, 2007.

Haeffelin, M., Bergot, T., Elias, T., Tardif, R., Carrer, D., Chazette, P., Colomb, M., Drobinski, P., Dupont, E., Dupont, J.-C., Gomes, L., Musson-Genon, L., Pietras, C., Plana-Fattori, A., Protat, A., Rangognio, J., Raut, J.-C., Rémy, S., Richard, D., Sciare, J., and Zhang, X.: Parisfog: Shedding new Light on Fog Physical Processes, Bulletin of the American Meteorological Society, 91, 767–783, https://doi.org/10.1175/2009BAMS2671.1, publisher: American Meteorological Society Section: Bulletin of the American Meteorological Society, 2010.

Heldens, W., Burmeister, C., Kanani-Sühring, F., Maronga, B., Pavlik, D., Sühring, M., Zeidler, J., and Esch, T.: Geospatial input data for the PALM model system 6.0: model requirements, data sources, and processing, Geoscientific Model Development Discussions, pp. 1–62, 2020.

Hersbach, H., Bell, B., Berrisford, P., Horányi, A., Sabater, J. M., Nicolas, J., Radu, R., Schepers, D., Simmons, A., Soci, C., and Dee, D.: Global reanalysis: goodbye ERA-Interim, hello ERA5, ECMWF newsletter, 159, 17–24, 2019.

Huang, H.-Y. and Margulis, S. A.: Impact of soil moisture heterogeneity length scale and gradients on daytime coupled land-cloudy boundary layer interactions, Hydrological Processes, 27, 1988–2003, iSBN: 0885-6087 Publisher: Wiley Online Library, 2013.

Hume, T.: Fog at New Zealand Airports: A Thesis Submitted to the Victoria University of Wellington in Fulfilment of the Requirements for the Degree of Doctor of Philosophy in Geophysics, Ph.D. thesis, Victoria University of Wellington, 1999.

Justice, C. O., Townshend, J. R. G., Vermote, E. F., Masuoka, E., Wolfe, R. E., Saleous, N., Roy, D. P., and Morisette, J. T.: An overview of MODIS Land data processing and product status, Remote Sensing of Environment, 83, 3–15, https://doi.org/10.1016/S0034-4257(02)00084-6, 2002.

Kadasch, E., Sühring, M., Gronemeier, T., and Raasch, S.: Mesoscale nesting interface of the PALM model system 6.0, Geoscientific Model Development, 14, 5435–5465, 2021.

Kessler, E.: On the distribution and continuity of water substance in atmospheric circulations, in: On the distribution and continuity of water substance in atmospheric circulations, pp. 1–84, Springer, 1969.

Landcare Research: NZDEM South Island 25 metre, https://lris.scinfo.org.nz/layer/48127-nzdem-south-island-25-metre/, 2018.

Landcare Research: LCDB v5.0 - Land Cover Database version 5.0, Mainland New Zealand, https://lris.scinfo.org.nz/layer/104400-lcdb-v50-land-cover-database-version-50-mainland-new-zealand/, 2020.

Lin, D., Khan, B., Katurji, M., Bird, L., Faria, R., and Revell, L. E.: WRF4PALM v1. 0: a mesoscale dynamical driver for the microscale PALM model system 6.0, Geoscientific Model Development, 14, 2503–2524, https://doi.org/https://doi.org/10.5194/gmd-14-2503-2021, 2021.

Lin, D., Katurji, M., Revell, L. E., Khan, B., Osborne, N., Soltanzadeh, I., and Kremser, S.: Fog type classification using a modified Richardson number for Christchurch, New Zealand, International Journal of Climatology, 2022.

Macara, G. R.: The climate and weather of Canterbury, NIWA, Taihoro Nukurangi, 2016.

https://doi.org/10.5194/egusphere-2022-1229
Preprint. Discussion started: 6 December 2022
© Author(s) 2022. CC BY 4.0 License.

Maronga, B. and Bosveld, F.: Key parameters for the life cycle of nocturnal radiation fog: a comprehensive large-eddy simulation study, Quarterly Journal of the Royal Meteorological Society, 143, 2463–2480, 2017.

Maronga, B., Hartogensis, O. K., Raasch, S., and Beyrich, F.: The effect of surface heterogeneity on the structure parameters of temperature and specific humidity: A large-eddy simulation case study for the LITFASS-2003 experiment, Boundary-layer meteorology, 153, 441–470, iSBN: 1573-1472 Publisher: Springer, 2014.

Maronga, B., Gryschka, M., Heinze, R., Hoffmann, F., Kanani-Sühring, F., Keck, M., Ketelsen, K., Letzel, M. O., Sühring, M., and Raasch, S.: The Parallelized Large-Eddy Simulation Model (PALM) version 4.0 for atmospheric and oceanic flows: model formulation, recent developments, and future perspectives, Geoscientific Model Development, 8, 2515–2551, https://doi.org/10.5194/gmd-8-2515-2015, 2015.

Maronga, B., Banzhaf, S., Burmeister, C., Esch, T., Forkel, R., Fröhlich, D., Fuka, V., Gehrke, K. F., Geletič, J., Giersch, S., et al.: Overview of the PALM model system 6.0, Geoscientific Model Development, 13, 1335–1372, 2020.

Mason, J.: The Physics of Radiation Fog, Journal of the Meteorological Society of Japan. Ser. II, 60, 486–499, https://doi.org/10.2151/jmsj1965.60.1_486, 1982.

Mazoyer, M., Lac, C., Thouron, O., Bergot, T., Masson, V., and Musson-Genon, L.: Large eddy simulation of radiation fog: impact of dynamics on the fog life cycle, Atmospheric Chemistry and Physics, 17, 13 017–13 035, 2017.

Meng, L. and Quiring, S. M.: A Comparison of Soil Moisture Models Using Soil Climate Analysis Network Observations, Journal of Hydrometeorology, 9, 641–659, https://doi.org/10.1175/2008JHM916.1, 2008.

New Zealand Meteorological Service: The Climatology of Christchurch International Airport, Tech. rep., The Service, Wellington, N.Z, volume: 171 (3) Report, 1982.

Osborne, N.: An Investigation into the Clearing Time of Stratus or Fog at Christchurch International Airport, with the Use of an Acoustic Sodar, A Thesis Submitted to the Victoria University of Wellington in Fulfilment of the Requirements for the Diploma of Applied Science (Meteorology), 2002.

Resler, J., Krč, P., Belda, M., Juruš, P., Benešová, N., Lopata, J., Vlček, O., Damašková, D., Eben, K., Derbek, P., Maronga, B., and Kanani-Sühring, F.: PALM-USM v1.0: A new urban surface model integrated into the PALM large-eddy simulation model, Geoscientific Model Development, 10, 3635–3659, https://doi.org/10.5194/gmd-10-3635-2017, publisher: Copernicus GmbH, 2017.

Rihani, J. F., Chow, F. K., and Maxwell, R. M.: Isolating effects of terrain and soil moisture heterogeneity on the atmospheric boundary layer: Idealized simulations to diagnose land-atmosphere feedbacks, Journal of Advances in Modeling Earth Systems, 7, 915–937, iSBN: 1942-2466 Publisher: Wiley Online Library, 2015.

Roux, B., Potts, R., Siems, S., and Manton, M.: Towards a better understanding of fog at Perth Airport, Journal of Hydrology, 600, 126 516, https://doi.org/10.1016/j.jhydrol.2021.126516, 2021.

Roy, D. P., Wulder, M. A., Loveland, T. R., C.e., W., Allen, R. G., Anderson, M. C., Helder, D., Irons, J. R., Johnson, D. M., Kennedy, R., Scambos, T. A., Schaaf, C. B., Schott, J. R., Sheng, Y., Vermote, E. F., Belward, A. S., Bindschadler, R., Cohen, W. B., Gao, F., Hipple, J. D., Hostert, P., Huntington, J., Justice, C. O., Kilic, A., Kovalskyy, V., Lee, Z. P., Lymburner, L., Masek, J. G., McCorkel, J., Shuai, Y., Trezza, R., Vogelmann, J., Wynne, R. H., and Zhu, Z.: Landsat-8: Science and product vision for terrestrial global change research, Remote Sensing of Environment, 145, 154–172, https://doi.org/10.1016/j.rse.2014.02.001, 2014.

Schwenkel, J. and Maronga, B.: Large-eddy simulation of radiation fog with comprehensive two-moment bulk microphysics: impact of different aerosol activation and condensation parameterizations, Atmospheric Chemistry and Physics, 19, 7165–7181, 2019.

https://doi.org/10.5194/egusphere-2022-1229
Preprint. Discussion started: 6 December 2022
© Author(s) 2022. CC BY 4.0 License.

Shao, Y., Liu, S., Schween, J. H., and Crewell, S.: Large-Eddy Atmosphere–Land-Surface Modelling over Heterogeneous Surfaces: Model Development and Comparison with Measurements, Boundary-Layer Meteorology, 148, 333–356, https://doi.org/10.1007/s10546-013-9823-0, 2013.

Sinergise Ltd: EO Browser, https://apps.sentinel-hub.com/eo-browser/, 2022a.

Sinergise Ltd: Sentinel Hub, https://www.sentinel-hub.com, 2022b.

Skamarock, W. C., Klemp, J. B., Dudhia, J., Gill, D. O., Liu, Z., Berner, J., Wang, W., Powers, J. G., Duda, M. G., Barker, D. M., and Huang, X.-Y.: A description of the advanced research WRF model version 4, National Center for Atmospheric Research: Boulder, CO, USA, p. 165, 2021.

Smith, D. K., Renfrew, I. A., Dorling, S. R., Price, J. D., and Boutle, I. A.: Sub-km scale numerical weather prediction model simulations of radiation fog, Quarterly Journal of the Royal Meteorological Society, 147, 746–763, 2020.

Sohrabinia, M., Rack, W., and Zawar-Reza, P.: Soil moisture derived using two apparent thermal inertia functions over Canterbury, New Zealand, Journal of Applied Remote Sensing, 8, 083 624, iSBN: 1931-3195 Publisher: SPIE, 2014.

Srivastava, A., Kumari, N., and Maza, M.: Hydrological Response to Agricultural Land Use Heterogeneity Using Variable Infiltration Capacity Model, Water Resources Management, 34, 3779–3794, https://doi.org/10.1007/s11269-020-02630-4, 2020.

Steeneveld, G. J., Ronda, R. J., and Holtslag, A. A. M.: The challenge of forecasting the onset and development of radiation fog using mesoscale atmospheric models, Boundary-Layer Meteorology, 154, 265–289, iSBN: 1573-1472 Publisher: Springer, 2015.

Stull, R. B.: Practical Meteorology: An Algebra-based Survey of Atmospheric Science, University of British Columbia, 2017.

Sturman, A. P. and Tapper, N. J.: The weather and climate of Australia and New Zealand, Oxford University Press, USA, 2006.

Tardif, R. and Rasmussen, R. M.: Event-based climatology and typology of fog in the New York City region, Journal of Applied Meteorology and Climatology, 46, 1141–1168, 2007.

Van Schalkwyk, L. and Dyson, L. L.: Climatological characteristics of fog at Cape Town International airport, Weather and Forecasting, 28, 631–646, 2013.

Vosper, S., Carter, E., Lean, H., Lock, A., Clark, P., and Webster, S.: High resolution modelling of valley cold pools, Atmospheric Science Letters, 14, 193–199, iSBN: 1530-261X Publisher: Wiley Online Library, 2013.

Vosper, S. B., Hughes, J. K., Lock, A. P., Sheridan, P. F., Ross, A. N., Jemmett-Smith, B., and Brown, A. R.: Cold-pool formation in a narrow valley, Quarterly Journal of the Royal Meteorological Society, 140, 699–714, iSBN: 0035-9009 Publisher: Wiley Online Library, 2014.

WMO: International meteorological vocabulary, 1992, Tech. rep., WMO/OMM/IMGW, 182, Geneva, 1992.